



1 **Tectono-thermal evolution of Oman's Mesozoic passive 2 continental margin under the obducting Semail Ophiolite: a 3 case study Jebel Akhdar, Oman**

4 Arne Grobe^{1,2}, Christoph von Hagke¹, Ralf Littke², István Dunkl³, Franziska Wübbeler¹,
5 Philippe Muchez⁴, Janos L. Urai¹

6 ¹Structural Geology, Tectonics, and Geomechanics, EMR Group, RWTH Aachen University, Germany

7 ²Geology and Geochemistry of Petroleum and Coal, EMR Group, RWTH Aachen University, Germany

8 ³Sedimentology & Environmental Geology, Geoscience Center Georg-August-Universität Göttingen, Germany

9 ⁴Geodynamics and Geofluids Research Group, Department of Earth and Environmental Sciences, KU Leuven,
10 Belgium

11 Correspondence to: Arne Grobe, arne.grobe@rwth-aachen.de, ORCID: 0000-0001-6471-0624

12 Keywords: basin modeling, passive margin, obduction, burial, Raman spectroscopy, thermochronology, thermal
13 maturity

14

15 **Abstract.** The Mesozoic sequences of the Oman Mountains experienced only weak post-obduction overprint and
16 deformation, thus they offer a unique natural laboratory to study obduction. We present a study of the pressure and
17 temperature evolution in the passive continental margin under the Oman Ophiolite, using numerical basin models
18 calibrated with thermal maturity data, fluid inclusion thermometry and low-temperature thermochronology.

19 Thermal maturity data from the Adam Foothills constrain burial in the foredeep moving in front of the advancing
20 nappes to be at least 4 km. Peak temperature evolution in the carbonate platform under the ophiolite is only weakly
21 dependent on the temperature of the overriding nappes which have cooled during transport from the oceanic
22 subduction zone to emplacement. Fluid-inclusion thermometry yields pressure-corrected homogenization
23 temperatures of 225 to 266 °C for veins formed during progressing burial, 296–364 °C for veins related to peak
24 burial and 184 to 213 °C for veins associated with late-stage strike-slip faulting. In contrast, the overlying
25 Hawasina nappes have not been heated above c. 170 °C, as witnessed by only partial resetting of the zircon (U–
26 Th/He thermochronometer).

27 In combination with independently determined temperatures from solid bitumen reflectance, we infer that the fluid
28 inclusions of peak-burial-related veins formed at minimum pressures of 225–285 MPa. This implies that the rocks
29 of the future Jebel Akhdar Dome were buried under 8–10 km of ophiolite on top of 2 km of sedimentary nappes,
30 which is in agreement with thermal maturity data of solid bitumen reflectance and Raman spectroscopy.

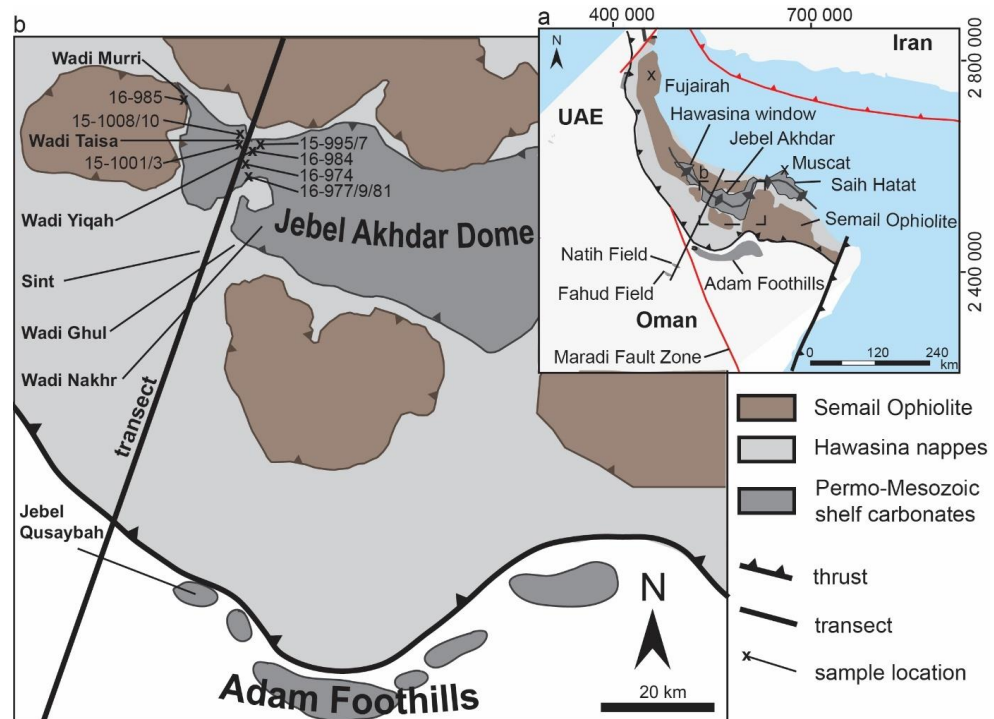
31 Burial of the passive margin under the ophiolite results in sub-lithostatic pore pressures, in agreement with
32 observations on veins formed in dilatant fractures in the carbonates. We infer that overpressure is induced by rapid
33 burial under the ophiolite nappes. Obduction-related tilt of the passive margin in combination with overpressure
34 in the passive margin caused fluid migration towards the south in front of the nappes.

35 Exhumation of the Jebel Akhdar as indicated by our zircon (U–Th)/He data, integrated with existing data, started
36 as early as the late Cretaceous to early Cenozoic, linked with extension along a major listric shear zone with top-
37 to-NNE shear sense, together with an early phase of extensional dome formation. The carbonate platform and
38 obducted nappes of the whole Jebel Akhdar cooled together below c. 170 °C between 50 and 40 Ma, before the
39 final stage of anticline formation.

40 **1. Introduction**

41 The Permo-Mesozoic platform sediments of northern Oman (Figure 1; e.g. Beurrier et al., 1986; Glennie et al.,
 42 1974; Lippard et al., 1982) with hydrocarbon accumulations in the southern foreland of the Jebel Akhdar Dome
 43 (Figures 1 and 2) are overlain by the Semail ophiolite nappe complex, the largest and best-preserved ophiolite on
 44 Earth. Limited tectonic extension after obduction followed by uplift, folding and deep erosion and the present day
 45 arid climate formed exceptional exposures in three tectonic windows and in the foreland fold-and-thrust belt of
 46 the Oman Mountains (Figure 1). The Oman Mountains have been investigated in many studies focusing on tectonic
 47 history (Breton et al., 2004; Cooper et al., 2014; Glennie et al., 1973, 1974; Grobe et al., 2018; Loosveld et al.,
 48 1996; Searle, 2007), stratigraphic sequences (Van Buchem et al., 2002; Grelaud et al., 2006; Homewood et al.,
 49 2008), geodynamic modelling (Duretz et al., 2015), hydrocarbon source rocks (Van Buchem et al., 1996; Philip et
 50 al., 1995; Scott, 1990) and reservoir rocks (Arndt et al., 2014; De Keijzer et al., 2007; Koehler et al., 2011; Virgo
 51 et al., 2013). Less well known is the temperature evolution of the sub-thrust sedimentary basin and the subsequent
 52 cooling history of the Jebel Akhdar (Aldega et al., 2017; Grobe et al., 2018; Hansman et al., 2017; Poupeau et al.
 53 1998; Saddiqi et al., 2006). A better understanding of this would further constrain the dynamics of obduction.

54



55

56

57 **Figure 1:** a) Tectonic setting of the Oman Mountains. Shaded in gray are the three tectonic windows of Hawasina, Jebel
 58 Akhdar and Saih Hatat as well as the Adam Foothills. Brown areas show the exposed Semail Ophiolite, black lines
 59 denote the obduction fronts of Semail and Masirah ophiolites, red lines denote lithosphere-scale structures. The modeled
 60 transect (black line) crosscuts the Jebel Akhdar window and continues to the Natih and Fahud oil fields in the
 61 southwestern mountain foreland. b) Geologic map of the Jebel Akhdar window with the location of the modeled transect
 62 (solid black line) and the locations of thermal maturity data (x).

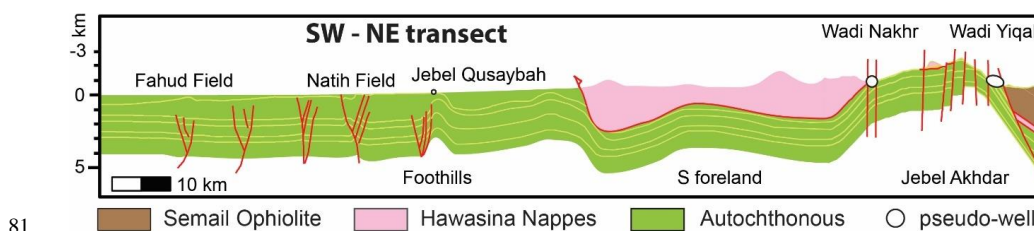


63 The full Permo-Mesozoic sequence of the carbonate platform below the ophiolite is well exposed, providing
64 outcrop samples to study the pressure and temperature history of this rapidly buried passive-margin sequence.
65 In other orogens, peak temperatures related to nappe emplacement were reconstructed by analyzing thermal
66 maturity of finely dispersed organic material (e.g. Teichmüller and Teichmüller, 1986; Eastern Alps: Lünsdorf et
67 al., 2012; Southern Alps: Rantitsch and Rainer, 2003; Apennines: Reutter et al., 1988). However, the number of
68 studies of thermal and pressure effects on overthrust sedimentary basins is limited and modeling approaches to
69 reconstruct such large scale overthrusts are rare (e.g. Deville and Sassi, 2006; Ferreiro Mähmann, 2001; Oxburgh
70 and Turcotte, 1974; Roure et al., 2010; Wygrala, 1989). In these studies, a main difficulty is to differentiate
71 between temperature history of obduction and overprinting in later phases of orogeny. In the Oman Mountains,
72 peak temperatures reached by obduction have not been overprinted, and fluid migration in the thrust belt is
73 predominantly related to obduction.

74

75 In this paper we present new thermal maturity, thermochronology and fluid inclusion data, and model the pressure-
76 temperature evolution of a transect across the entire Jebel Akhdar extending from the undeformed passive margin
77 sequence in the south to the Batinah coast in the north (Figure 2). This allows to better constrain temperature and
78 pressure conditions of deepest burial as well as the time of dome formation and exhumation which is linked to the
79 structural and tectonic evolution of the area.

80



81
82 **Figure 2:** Structural transect used for modeling of the Jebel Akhdar Dome and its southern foreland (compiled from
83 Al-Lazki et al., 2002; Filbrandt et al., 2006; [Caron et al., 2007](#); Warburton et al., 1990). Highlighted are the locations of the
84 pseudo-wells (white circles, size depict areal sample interpolation) in Wadi Nakhr, Wadi Yiqah and at Jebel
85 Qusaybah, Adam Foothills, which were used for model calibration.

86 2. Geological setting

87 2.1. Tectonic setting

88 Along the northeastern coast of Arabia, the NW-SE oriented Oman Mountains form a more than 400 km long
89 anticlinal orogen (Figure 1). The mountain belt consists of allochthonous sedimentary and ophiolitic nappes thrust
90 onto a Permo-Mesozoic passive continental margin (Breton et al., 2004; Glennie et al., 1973; Loosveld et al., 1996;
91 Searle and Cox, 2002).

92 This margin was formed during opening of the Neotethyan ocean (e.g. Loosveld et al., 1996) and the Permo-
93 Mesozoic Hawasina Basin (Béchenne et al., 1988; Bernoulli et al., 1990). Cretaceous convergence of Arabia and
94 Iran inverted the rifting and initiated subsea thrusting of the later Semail Ophiolite on top of the Arabian Plate at
95 97-92 Ma, as recorded by U-Pb geochronology (Roux et al., 2013, 2016; Warren et al., 2005) and $^{40}\text{Ar}/^{39}\text{Ar}$ dating
96 of the metamorphic sole (Hacker et al., 1996). Obduction initiation and the advancing ophiolite resulted in a
97 flexural forebulge that moved southwestwards through the passive margin during the Upper Cretaceous



98 (Robertson, 1987). Forebulge migration induced up to 1100 m of uplift of the Permo-Mesozoic Arabian Platform
99 and erosion of the Cretaceous platform sediments (Searle, 2007). In the field this can be observed at the Wasia-
100 Aruma Break (e.g. Robertson, 1987).

101 During northeastward directed subduction of the Arabian margin, parts of the Hawasina ocean sediments and
102 volcanics detached and became accreted in front and beneath the ophiolite nappe (Béchennec et al., 1988, 1990;
103 Glennie et al., 1974; Searle et al., 2003; Warburton et al., 1990). Palinspastic reconstructions of the Hawasina
104 Nappes locate the position of the initial ophiolite thrusting 300-400 km offshore the Arabian coast (Béchennec et
105 al., 1988; Glennie et al., 1974). 

106 Burial under the allochthonous sequences led to the formation of three crack-seal calcite vein generations in the
107 margin sequence, which represent overpressure build-ups and releases (Gomez-Rivas et al., 2014; Grobe et al.,
108 2018; Hilgers et al., 2006; Holland et al., 2009; Virgo, 2015). Peak metamorphism of the subducted margin is
109 recorded by eclogites exposed in the As Sifah region (E-Saih Hatat, Figure 1a), where the burial triggered thermal
110 climax resulted in zircon and rutile  stalling at c. 79 Ma (Warren et al., 2003). 

111 The sedimentary record in the Batil coast and the foreland, as well as laterite formation on top of the ophiolite 
112 suggest that obduction slowed or stopped in the early Paleogene, and the ophiolite was exposed subaerially
113 (Coleman, 1981; Forbes et al., 2010; Nolan et al., 1990). This slowdown might relate to the formation of the
114 Makran subduction zone at c. 35 Ma (Figure 1; Agard et al., 2005; Hassanzadeh and Wernicke, 2016; Jacobs et
115 al., 2015; Mouthereau, 2011). This shift of deformation to the north resulted in preservation of the initial stage of
116 the obduction orogen in northern Oman. 

117 Regional post-obduction extension took place along ductile top-to-NNE shear zones, dated to 64 ± 4 Ma (Hansman
118 et al., 2018), followed by NW-SE striking normal fault systems (Al-Wardi and Butler, 2007; Fournier et al., 2006;
119 Grobe et al., 2018; Hanna, 1990; Hilgers et al., 2006; Holland et al., 2009; Loosveld et al., 1996; Mattern and
120 Scharf, 2018; Virgo, 2015). Renewed Arabia-Eurasia convergence during the Cenozoic formed the three dome
121 structures with the associated tectonic windows. Timing of formation and exhumation of the Jebel Akhdar Dome
122 is still debated. Stratigraphic arguments for a late Cretaceous doming are Maastrichtian rocks unconformably
123 deposited on Hawasina (Bernoulli et al., 1990; Fournier et al., 2006; Hanna, 1990; Nolan et al., 1990), while
124 inclined Miocene strata at the northern fringes of the dome points to a younger Miocene doming (Glennie et al.,
125 1973). Consequently, some models suggest a two-phased exhumation in Cretaceous and Miocene (Searle, 1985,
126 2007), in agreement with structural observations suggesting early dome formation and later amplification of the
127 structure (Grobe et al., 2018). 

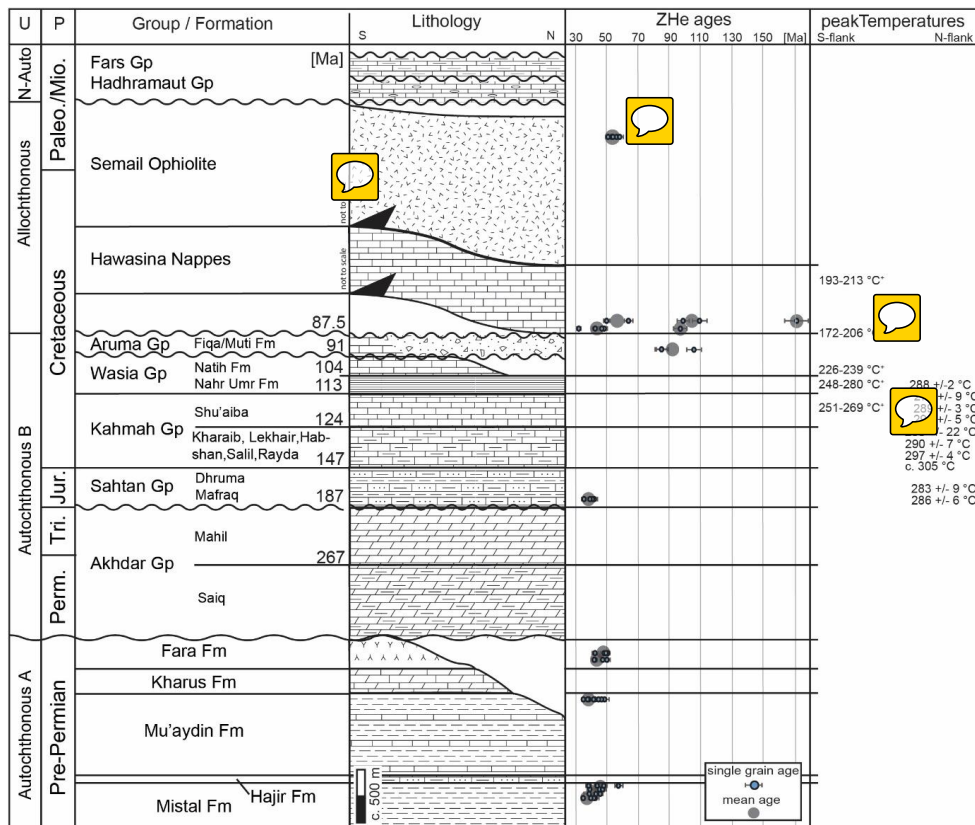
128 Thermochronological constraints for the exhumation of the Jebel Akhdar Dome from samples below and above
129 the carbonate platform were reported (Hansman et al., 2017; Mount et al., 1998; Poupeau et al., 1998; Saddiqi et
130 al., 2006). Earlier studies argue for two-stage cooling with reheating in late Miocene (Poupeau et al., 1998; Saddiqi et
131 al., 2006). More recent studies, however, have shown that the data of Poupeau et al. (1998) and Saddiqi et al.
132 (2006) can also be explained by a cooling-only scenario with exhumation in the Eocene (Hansman et al., 2017). 

133 **2.2. Stratigraphic sequence**

134 Sediments in the Jebel Akhdar area consist of a pre-Permian sequence (Autochthonous A, Figure 3) unconformably
135 overlain by a Permo-Mesozoic sequence (Autochthonous B, Figure 3; Beurrier et al., 1986; Breton et al., 2004;
136 Glennie et al., 1974; Rabu et al., 1990). During the late Cretaceous, Hawasina nappes and the Semail Ophiolite



137 were emplaced onto the passive margin, and neo-autochthonous rocks of Cenozoic age were deposited on top of
 138 the ophiolite after obduction (Béchennec et al., 1988; Forbes et al., 2010; Loosveld et al., 1996).
 139



140
 141 Figure 3: Stratigraphy of the Jebel Akhdar area with its two passive margin sequences Autochthonous A and B
 142 overthrust by Hawasina and Semail Nappes and unconformably overlain by neo-autochthonous units (Figure 1). Ages
 143 (Forbes et al. 2010) are basin modeling input data. In addition, thermal calibration data is shown: ZHe ages
 144 (Table 2) show two different grain age populations. Maximum burial temperatures from organic matter maturity (bl) Table
 145 1) outline the temperature increase with stratigraphic depth. Temperature data was supplemented by values from
 146 *Mozafari et al. (2015) and *Grobe et al. (2016). (U = Unit, P = Period). Note that the Semail and Hawasina nappes are
 147 shown in their structural rather than stratigraphic positions. Data is compiled from Beurrier et al. (1986), Loosveld et
 148 al. (1996), Terken et al. (2001) and Forbes et al. (2010).

149 Autochthonous A deposits are exposed in the Jebel Akhdar window down to the Mistal Fm. (Beurrier et al., 1986).
 150 Black limestones of the Hajir Fm., mudstone rich carbonate beds of the Mu'aydin Fm. and lime- and dolostones
 151 of the Kharus Fm. conformably overlie the Mistal Fm. (Beurrier et al., 1986; Glennie et al., 1974). Platform break-
 152 up is recorded by laminated cherts and volcanoclastics of the Fara Fm. (Beurrier et al., 1986) followed by an
 153 unconformity representing a gap from Cambrian to Permian times (Loosveld et al., 1996). After establishment of
 154 the Neotethyan Ocean during the Permian, northern Oman returned to stable passive margin conditions and the
 155 carbonate platform of the Autochthonous B developed, with the Akhdar Gp. at its base (Koehler et al., 2010;
 156 Pöppelreiter et al., 2011). This is unconformably overlain by limestones with clastic interlayers of the Jurassic
 157 Saftan Gp. (Beurrier et al., 1986; Pratt et al., 1990). Limestones with marly, frequently organic-rich intercalations
 158 of the Cretaceous Kahmah (Habsi et al., 2014; Vahrenkamp, 2010) and Wasia groups (Grelaud et al., 2006;



159 Homewood et al., 2008; Philip et al., 1995) form the youngest platform sediments (Robertson, 1987; Warburton
160 et al., 1990).

161 The obduction-related moving forebulge and associated uplift ended passive margin deposition and eroded the
162 topmost Wasia Gp. (Natih Fm.) in the Jebel Akhdar (Figure 3), and deeper in the Saih Hatat region. Deposition in
163 the foredeep basins in front and behind the forebulge was dominated by the syn- and postorogenic, conglomerate-
164 rich sediments of the Muti Fm., Aruma Gp. (Beurrier et al., 1986; Robertson, 1987). Towards the south, in the
165 Adam Foothills, this laterally grades to calcareous foreland sediments of the Fiqa Fm. (Forbes et al., 2010;
166 Robertson, 1987; Warburton et al., 1990).

167 Hawasina sediments accreted in front and beneath the ophiolite represent marine slope and basin facies, time
168 equivalent to the Autochthonous B (Béchennec et al., 1990). After obduction of oceanic crust on top of the passive
169 margin, neo-autochthonous evaporites and carbonates of the Paleocene to Eocene Hadhramaut Gp. and bivalve-
170 rich dolomites and limestones of the Oligo- to Pliocene Fars Gp. were deposited south of the mountains
171 (Béchennec et al., 1990; Forbes et al., 2010). Paleogeographical reconstructions show the Oman Mountains had
172 high relief after obduction, followed by a low relief landscape until the early Eocene (Nolan et al., 1990). In the
173 middle Eocene marine transgression caused widespread deposition of limestones, as witnessed e.g. by the Seeb
174 and Ruwaydah Formations (Nolan et al., 1990). Post Eocene times show renewed relief development and
175 continued uplift until recent times (Glennie et al., 1974; Searle, 2007).

176 **2.3. Temperature evolution of the Autochthon**

177 Only limited paleo-temperature data is available from the carbonate platform. Peak-burial temperatures of 226-
178 239 °C for the top of the platform were measured using solid bitumen reflectance and Raman spectroscopy of
179 carbonaceous material (RSCM) in the Jebel Akhdar (Grobe et al., 2016). Vein crystallization temperatures of 166-
180 205 °C at the top of the Natih A (near Al Hamra) were measured by quartz-calcite thermometry in veins formed
181 during ophiolite-induced burial (Gen. III of Grobe et al., 2018), and approximately 255 °C for veins associated
182 with a later normal fault network (Gen V of Grobe et al., 2018; Stenhouse, 2014). Fluid inclusions (FI) of bedding
183 parallel pinch-and-swell veins (top-to-NNE shear after peak burial, Gen. IV of Grobe et al., 2018) show
184 uncorrected minimum trapping temperatures of 134-221 °C in the lower beds of the Sahtan Group at Wadi Nakhr
185 (Holland et al., 2009). Reflectance measurements of solid-bitumen-containing veins in the Wadi Ghul (Gen I of
186 Grobe et al., 2018), which are interpreted to be associated with fluid mobilization during forebulge migration,
187 showed maximum temperatures of 230 °C (Fink et al., 2015).

188 Reconstructions of the thermal history using numerical basin modeling were presented for the southern foreland
189 and the contained Natih Fm. outlining its extreme efficiency interpreted to be a result of thrusting-induced lateral
190 migration (Terken, 1999; Terken et al., 2001) and the Proterozoic hydrocarbon source rocks (Visser, 1991).



191 **2.4. Temperature evolution of the Semail Ophiolite nappe / Allochthon**

192 Initial intra-oceanic ophiolite thrusting and associated metamorphism at its sole took place at peak temperatures
193 of 840 ± 70 °C at 97-92 Ma measured at several locations in the Oman Mountains (Gnos and Peters, 1993; Hacker
194 and Mosenfelder, 1996; Rioux et al., 2013; Searle and Cox, 2002; Warren et al., 2003). At 90-85 Ma the base of
195 the ophiolite cooled to 350 ± 50 °C (white mica Ar/Ar dating, Gnos and Peters, 1993). At around 80 Ma the deepest
196 burial of the Oman margin beneath the ophiolite was reached (Hacker and Mosenfelder, 1996; Warren et al., 2005)
197 with temperatures in the metamorphic sole below 300 °C (Le Metour et al., 1990; Saddiqi et al., 2006). Due to the



198 at least 2 km thick imbricated Hawasina Nappes between the ophiolite and the passive margin sequence, the
199 thermal overprint of the nappe temperature on the top of the carbonate platform was low. Limited thermal
200 overprinting of the units underlying the ophiolite is supported by the fact that the sediments of the nappes directly
201 below the ophiolite do not show signs of regional metamorphism in the Jebel Akhdar region (Searle, 1985). A
202 lithospheric scale thermo-mechanical model of the thrusting in northwestern Oman includes a thermal anomaly
203 c. 100 km northwest offshore the Arabian margin to initiate subsea thrusting (Duretz et al. 2015). 

204 **2.5. Petroleum system elements**

205 Several petroleum systems developed in the carbonate platform of northern Oman with important source rock
206 horizons in the Natih Fm. (Natih Members B and E). Both members contain Type I/II kerogen with total organic
207 carbon contents up to 15 % in the Natih B and up to 5 % in the Natih E, respectively (Terken, 1999). Ophiolite
208 obduction in northern Oman led to over-mature Natih source rocks (Grobe et al., 2016). However, the thermal
209 impact of the moving forebulge and the importance of tectonic processes for fluid migration below and in front of
210 the obduction orogen are not clear. At least three different generations of solid bitumen particles in veins and
211 source rocks on the southern slope of the Jebel Akhdar suggest pulses of hydrocarbon generation and migration in
212 front of the Oman Mountains (Fink et al., 2015; Grobe et al., 2016). In central Oman, Shu'aiba and Tuwaiq oils
213 are produced out of Kahmah and Sahtan Gp. reservoirs, sealed by argillaceous shales of the Nahr Umr Fm. (Terken
214 et al., 2001). These units are all well-exposed in the Oman Mountains.

215 **3. Methods**

216 Samples for thermal reconstruction were collected during several field campaigns between 2013 and 2016 in the
217 Jebel Akhdar Dome (Figure 2). 

218 **3.1. Elemental analysis and thermal maturity**

219 To determine thermal maturity, over 100 dark, unweathered and organic-rich samples were taken from different
220 stratigraphic units in the Jebel Akhdar (Figure 3). Based on total organic carbon (TOC) content as determined by
221 Grobe et al., (2016), 13 samples were selected for thermal maturity analysis on surfaces cut perpendicular to
222 bedding. Results were used to calibrate peak-burial temperatures of the numerical basin models. The organic
223 particles lack sufficient size or surface quality for reflectance measurements and are therefore investigated by
224 confocal Raman spectroscopy of carbonaceous material. The technique measures vibrational energies of chemical
225 bonds which change during temperature induced reorganization of amorphous carbonaceous material (kerogen) to
226 graphite (e.g. Aoya et al., 2010; Beyssac et al., 2002; Kouketsu et al., 2014). Measurements were conducted at the
227 Geoscience Center, Göttingen, on a Horiba Jobin Yvon HR800 UV spectrometer attached to an Olympus BX-41
228 microscope and a 100× objective. A high-power diode laser with a wavelength of 488 nm and an output power of
229 50 mW was installed and a D1 filter avoided sample alteration by heating. Each spectral window (center at
230 1399.82 cm⁻¹, grid of 600 lines/mm) was measured 5 to 10 times for 2 to 10 seconds with a Peltier CCD detector
231 at activated intensity correction. For quality control, the 520.4 cm⁻¹ line of a Si-wafer was measured every 30
232 minutes without observable drift of the measurements. To transform the measured data into VR_r values the scaled
233 total area (STA) approach of Lünsdorf (2016) was applied with the equation of Grobe et al. (2016): 

$$VR_r = -\frac{STA - 280.13}{24.71} \quad [\%]$$



235 From VR_r calculations peak-burial temperatures were determined following the approach of Barker and Pawlewicz
236 (1994). For calibration of the numerical basin models, data was supplemented by thermal maturity and peak-burial
237 temperature data of 63 Natih B source rock samples, taken around the Jebel Akhdar Dome (Grobe et al., 2016),
238 and two data points in the Adam Foothills on Jebel Qusaybah (Mozafari et al., 2015).

239 **3.2. Fluid inclusion thermometry**

240 Doubly-polished wafers (c. 200 µm thick) of four vein samples (FI-N1, -N2, -M1, -M2) have been prepared
241 according to the procedure described by Muchez et al. (1994). Fluid inclusion (FI) petrography and thermometry
242 was performed to analyze the temperature-pressure conditions and fluid's salinity. FIs represent paleofluids
243 accidentally trapped in a crystalline or amorphous solid during mineralization, lithification or both (Diamond,
244 2003). If unaffected by later changes, trapping pressure and temperature is given by the homogenization
245 temperature (Barker and Goldstein, 1990). Based on the time of trapping primary (mineral growth), secondary
246 (fracture-related) and pseudosecondary inclusions are distinguished (Barker and Goldstein, 1990; Diamond, 2003;
247 Goldstein, 2001; Van Den Kerkhof and Hein, 2001):

248 Two calcite vein samples of the Natih Fm. (FI-N1 and 2, Locations Figure 4) represent conditions related to early
249 burial (FI-N2, structural generation I of Grobe et al. 2018), and burial beneath the ophiolite (FI-N1, structural
250 generation III of Grobe et al. 2018). Two quartz-rich calcite veins of the Muti Fm. (FI-M1 and 2, Locations Figure
251 4) are related to late, NE-SW striking strike slip faults (generation IX of Grobe et al. 2018). FI assemblages were
252 defined and fluid inclusions measured with a Linkam THMSG600 thermostage (accuracy ± 0.1 °C) attached to an
253 Olympus BX60 microscope at the KU Leuven, Belgium. Calibration was performed using CO₂, H₂O-NaCl, H₂O-
254 KCl, and H₂O standards. Homogenization temperatures (T_h) were measured prior to temperatures of complete
255 freezing (T_f), first melt (T_{fm}), and complete melting of ice (T_{m(ice)}) to avoid stretching or leakage due to the volume
256 increase during ice formation. All measured temperatures were recorded during heating, except of the freezing
257 temperature (T_f). Pressure corrections of T_h were conducted with the program FLINCOR (Brown, 1989) for
258 280 and 340 MPa, assuming 8 to 10 km of ophiolite overburden (see model results, ρ= c. 3070 kg/m³) and 2 km
259 of sedimentary Hawasina Nappes (ρ= c. 2450 kg/m³), and for 45 MPa, assuming 2°km of sedimentary overburden
260 (Al-Lazki et al., 2002; Grobe et al., 2016). Fluid salinities were calculated from the T_{m(ice)} values considering a
261 H₂O-NaCl composition (Bodnar, 1993), which is based on the T_{fm} values.

262 **3.3. Thermochronology**

263 Zircon (U-Th)/He (ZHe) dating allows to reconstruct the tectono-thermal history of the topmost few kilometers of
264 the Earth's crust. Helium retention in less metamict zircon crystals is sensitive in the temperature range between
265 c. 130 and 170 °C, i.e. the zircon partial retention zone (PRZ, Reiners, 2005). 11 rocks sampled above, below and
266 within the carbonate platform were selected for ZHe dating. Zircon crystals were released using high voltage pulse
267 crushing (<http://www.selfrag.com>) and concentrated by standard mineral separation processes (drying, dry sieving,
268 magnetic and heavy liquid separation). Three to eight clear, intact, euhedral single crystals were selected per
269 sample and transferred into platinum micro-capsules. They were degassed under high vacuum by heating with an
270 infrared diode and extracted gas purified using a SAES Ti-Zr getter at 450 °C. Helium was analyzed with a Hiden
271 triple-filter quadrupole mass spectrometer. Degassed zircons were subsequently dissolved in pressurized teflon
272 bombs, spiked and U, Th and Sm measured with a Perkin Elmer Elan DRC II ICP-MS equipped with an APEX
273 micro flow nebulizer.



274 Time-temperature histories were reconstructed using the HeFTy 1.8.3 software package (Ketcham, 2005) applying
275 kinetic zircon properties of Guenther et al. (2013). For samples with reset zircons the only constraint used was a
276 minimum temperature above 200 °C between deposition and the calculated ZHe age. Thermal modeling was
277 conducted until 100 statistically good time-temperature paths were achieved (goodness of fit: 0.5, value for
278 acceptable fit: 0.05). In cases where this was not possible, at least 10,000 independent paths were calculated.

279 **3.4. Numerical basin modeling**

280 Structural evolution was palinsastically reconstructed starting from the present-day profile using Move 2D
281 (2016.1, Midland Valley Exploration). Geometries and relative ages of the structures were supplemented with
282 subsurface data (Al-Lazki et al., 2002; Filbrandt et al., 2006; Searle et al., 2004; Warburton et al., 1990). The
283 reconstruction workflow was as follows: (1) faulted layers in the southern foreland were restored, (2) doming was
284 retro-deformed by vertical simple shear, before (3) normal faults in the Jebel Akhdar were restored. This sequence
285 is based on our tectonic model (Grobe et al., 2018). The resulting geometries were used as input for 2D PetroMod
286 2014.1 (Schlumberger) basin modeling, enabling thermal maturity reconstruction for vitrinite reflectance values
287 of 0.3 to 4.7 % by the use of the EASY % R_o approach (Sweeney and Burnham, 1990). The numerical basin model
288 is based on a conceptional definition of events. Based on this sequence of events (sedimentation, erosion, hiatus)
289 a forward, event-stepping modeling is performed, starting with the deposition of the oldest layer. For each event
290 lithologies and related petrophysical rock properties are assigned. The final basin model (representing the present
291 day) fits the geometries deduced from seismic interpretation and geology. ~~This is the first time that ophiolite~~
292 ~~obduction is reconstructed using a petroleum system modelling software such as PetroMod.~~ To simulate obduction
293 we used a rapid, stepwise-laterally-advancing emplacement, i.e. sedimentation, of ophiolitic rocks. This is
294 reasonable, as we will show that the ophiolite did not thermally overprint the passive margin sequence from above.
295 For our conceptual model the following sequence of events was implemented (Figure 3): (1) passive margin
296 carbonate sedimentation from Permian until late Cenomanian times (Forbes et al., 2010; Loosveld et al., 1996),
297 interrupted by a short erosional period at the Triassic-Jurassic boundary (Koehler et al., 2010; Loosveld et al.,
298 1996), (2) a moving forebulge associated with a paleo-water depth increase in its foredeep and erosion of the top
299 of the carbonate platform in the north of the transect (Wasia-Aruma break, 91-88.6 Ma, Robertson, 1987), (3) the
300 emplacement of allochthonous sedimentary nappes and (4) subsequent obduction, i.e. stepwise, rapid
301 sedimentation, of the ophiolite with deepest burial reached at c. 79 Ma (Warren et al., 2005). The area of the Adam
302 Foothills, represented in the transect by the Jebel Qusaybah, is a relic of the moving forebulge not overthrust by
303 allochthonous units – this was used to calibrate burial depth of the foredeep at this point in the transect. The south
304 of the foothills is unaffected by foredeep and obduction, but also lacks thermal calibration data. Absolute ages,
305 thicknesses, lithologies and related petrophysical properties as well as source rock properties were associated
306 according to results of our own field mapping and the compiled data from Forbes et al. (2010; Figure S1).
307 Thermal boundary conditions of the model have been defined for each time step by the basal heat flow (HF) and
308 the sediment water interface temperature (SWIT), representing the upper thermal boundary (Figure S2). To
309 account for active margin tectonic uplift and exhumation of the Jebel Akhdar, we assume an increase in basal
310 heat flow since the late Cretaceous. The resulting heat flow trend (Figure S2, Terken et al., 2001; Visser, 1991)
311 has been assigned to the entire transect. Paleo-surface temperatures were estimated based on Oman's paleo-latitude
312 (after Wygrala, 1989) corrected by the effect of the paleo-water depth (PWD) derived from the facies record (Van



313 Buchem et al., 2002; Immenhauser et al., 1999; Immenhauser and Scott, 2002; Koehler et al., 2010; Pratt et al.,
314 1990; Robertson, 1987).

315 This set-up has been iterated until modeling results fit the thermal calibration data (Table 1). Main uncertainties
316 derive from the unknown thickness of paleo-overburden (Muti Fm., Ophiolite, Hawasina Nappes) and uncertainty
317 of paleo-basal heat flow. Present-day heat flow was calibrated by data and borehole temperatures of Visser (1991)
318 and Rolandone et al. (2013) and peak-burial temperatures determined by Raman spectroscopy and solid bitumen
319 reflectance data (Table 1). From surface samples and their position in the stratigraphic column various pseudo-
320 wells were created (e.g. Nöth et al., 2001) and used as control points for the 2D model (Figure 2). The model was
321 used for sensitivity analyses of different input parameters.

322 **4. Results**

323 **4.1. Thermal maturity and host rock burial temperatures**

324 From Raman spectroscopy, integrated deformation peaks (D-peaks) give scaled total areas of 90-156 which
325 correspond to peak-burial temperatures of 266 to 300 °C (Grobe et al., 2016; Table 1). The maximum temperatures
326 increase with stratigraphic age and are similar on the northern and southern flanks of the Jebel Akhdar Dome (e.g.
327 Natih Fm.). Nahr Umr and Shu'aiba Fm. show slightly higher peak temperatures in the north of the transect (Figure
328 3). Temperature estimates based on RSCM and solid bitumen reflectance (Grobe et al., 2016) yielded similar
329 temperatures for the southern flank of 248-280 °C for the Nahr Umr, 226-239 °C for the Natih B and 172-206 °C
330 for the Muti, respectively (Table 1, Figure 3). Vitrinite reflectance data of Mozafari et al. (2015) shows
331 temperatures of c. 145-182 °C for Natih B in the Jebel Qusaybah, Adam Foothills, an area not overthrust by the
332 ophiolite complex.

333



sample No.	location			No. of measurements	mean D_STA	calculated VRi [%]	mean Temp.	
15_995	northern flank	Wadi Yiqah	Sahtan Gp.	M	14	113 +/- 14	6,52	286 +/- 6 °C
15_997		Wadi Yiqah	Shu'aiba	M	10	115 +/- 5	6,69	289 +/- 3 °C
15_1001		Wadi Taisa	Kh 2	M	1	78	8,19	305 °C
15_1003		Wadi Taisa	Kh 2	M	8	96 +/- 9	7,44	297 +/- 4 °C
15_1008		Wadi Taisa	top of Kh 2	M	8	113 +/- 15	6,78	290 +/- 7 °C
15_1010		Wadi Taisa	Shu'aiba	M	13	98 +/- 11	7,28	295 +/- 5 °C
15_1010		Wadi Taisa	Shu'aiba	P	4	149 +/- 15	5,31	270 +/- 9 °C
16_974		Tr- Jur fault	base Sahtan Gp.	P	6	125 +/- 17	6,29	283 +/- 9 °C
16_977		Kharb Plateau	base Natih Fm.	M	10	156 +/- 9	5,04	266 +/- 6 °C
16_979		Kharb Plateau	top Nahr Umr Fm.	M	2	117 +/- 4	6,60	288 +/- 2 °C
16_981		Kharb Plateau	top Nahr Umr Fm.	M	1	149	5,30	270 °C
16_984		Wadi Taisa	Kh 2	M	3	172 +/- 26	5,29	268 +/- 22 °C
16_985		Wadi Murri	Shu'aiba	M	2	90 +/- 4	7,69	300 +/- 2 °C
Grobe et al. (2016)_SV10	southern flank	Wadi Nakhr	Natih	P	6	-	2,83	227-231 °C
Grobe et al. (2016)_AG22		Wadi Nakhr	Natih	M	4	-	3,72	225-260 °C
Grobe et al. (2016)_AG01		Wadi Nakhr	Shu'aiba (Kh 3)	M	4	-	4,49	251-269 °C
Grobe et al. (2016)_AG11		Sint	Hawasina	P	5	-	2,45	193-213 °C
Grobe et al. (2016)_AG25		Balcony Walk Nakhr	Nahr Umr	M	4	-	4,23	226-267 °C
Grobe et al. (2016)_AG26_1		Balcony Walk Nakhr	Nahr Umr	P	2	-	(2.58)	(211-213 °C)
Grobe et al. (2016)_AG26_3		Balcony Walk Nakhr	Nahr Umr	M	2	-	4,96	275-280 °C
Grobe et al. (2016)_AG27		Balcony Walk Nakhr	Nahr Umr	M	3	-	4,61	248-266 °C
Grobe et al. (2016)_AG30		Balcony Walk Nakhr	Nahr Umr	M	3	-	4,25	248-257 °C
Grobe et al. (2016)_AG37		Jebel Shams	Muti	P	3	-	2,16	191-208 °C
Grobe et al. (2016)_AG38		Jebel Shams	Muti	P	2	-	1,99	172-206 °C
reference	location			No. of measured particles	measured BRi [%]	calculated / measured VRi [%]	calculated T _{burial} (Barker and Pawlewicz, 1994)	
Grobe et al. (2016)	South. fl.	Wadi Nakhr area	Natih B	BR _r	253	3.08-3.59	3.08-3.59	226-239 °C
Fink et al. (2015)		Wadi Nakhr area	Natih B	BR _r	200	3.10-3.14	-	c. 225 °C
Fink et al. (2015)		Wadi Nakhr area	Natih A Vein	BR _r	c. 250	3.40-3.76	-	-
Grobe et al. (2016)		Al Hamra area	Natih B	BR _r	20	2.95-3.34	2.95-3.34	223-233 °C
Grobe et al. (2016)	N	Wadi Sahtan	Natih B	BR _r	6	3,32	3,32	232 °C
Mozafari et al. (2015), measured at RWTH		Jebel Qusaybah	Natih B	VR _r	25	-	1,8	c. 182 °C
		Jebel Qusaybah	Natih B	VR _r	20	-	1,1	c. 145 °C



334

Table 1: Thermal maturity data and calculated peak temperatures of northern Oman. Temperatures from Raman spectroscopy of carbonaceous material are calculated based on the STA approach of Lünsdorf (2016) and the formula published by Grobe et al (2016). M/P indicate if measurement was conducted on solid bitumen particles (P) or below the surface of the matrix (M). Data of Mozafari et al. (2015) are used for Jebel Qusaybah, Adam Foothills.

335

336

337

338

339



340 **4.2. Thermochronology**

341 Results of the ZHe dating are shown in [figures 3](#)[Figure 3](#) and 4; time-temperature paths modeled with HeFTy are
342 included in the electronic supplement (Figures S3 and ). Samples from the carbonate platform (stratigraphically
343 older than Muti Fm.) have been entirely reset after deposition (Figure 3). This coincides with the center of the
344 Jebel Akhdar Dome in which all cooling ages fall in the range of 48.7 ± 1.8 to 39.8 ± 3.0 Ma (Table 2, Figure 4).
345 Sample T4, collected in the Muti Fm., yields an apparent mean age of 93.8 ± 6.9 Ma and samples T5 and T7 of
346 the Hawasina Nappes collected at the northern and the southern slope of the dome, show two grain age populations
347 of 43.0 ± 3.7 / 99.2 ± 8.5 Ma, and 58.9 ± 7.0 / 106.0 ± 5.2 Ma, respectively. In sample T5, an additional single
348 grain age population of 172.9 ± 14.9 Ma was obtained.

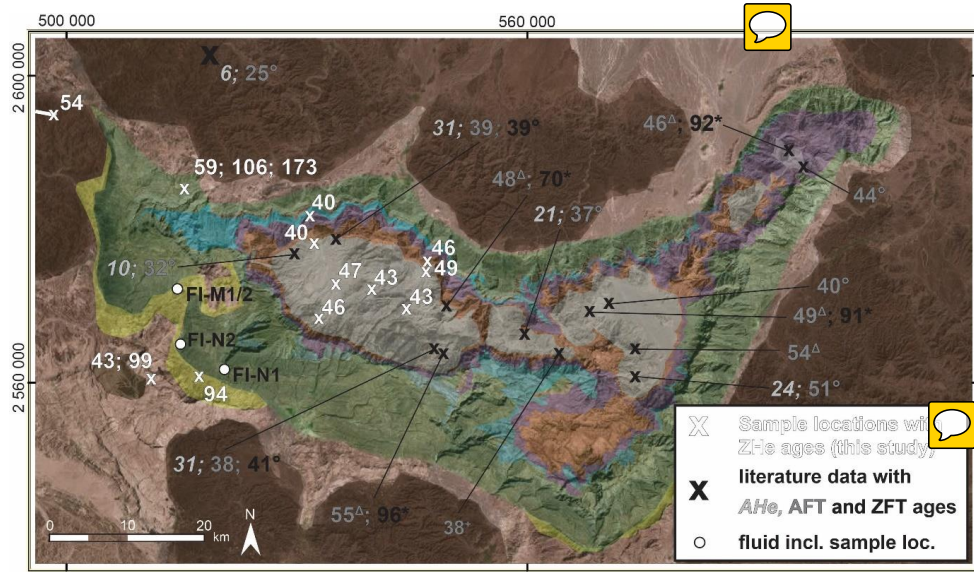
349



sample	lithology / location	He			²³⁸ U			²³² Th			Th/U	Sm			ejection correct. (Pt)	uncorr eacted	FT corrected	mean age [Ma]			
		vol. [ncc]	1 σ [%]	mass [ng]	1 σ [%]	conc. [ppm]	mass [ng]	1 σ [%]	conc. [ppm]	ratio		mass [ng]	1 σ [%]	conc. [ppm]				He age [Ma]	He age [Ma]	2 σ [%]	2 σ [Ma]
T1-21	sandstone		5,31	0,83	1,04	1,81	212,00	0,38	2,41	77,66	0,37	0,03	10,43	6,44	0,754	38,90	51,60	8,20	4,20		
T1-22	547533	2574875	6,05	0,84	1,31	1,81	323,34	0,33	2,41	80,49	0,25	0,01	21,24	2,97	0,737	36,10	49,10	8,70	4,30	48,70 +/- 1,80	
T1-23	Fara Fm.	Autochthon A	3,45	0,87	0,84	1,81	212,21	0,30	2,41	74,73	0,35	0,02	14,08	3,83	0,719	31,30	43,60	9,20	4,00		
T1-24			3,15	0,86	0,64	1,82	178,10	0,34	2,41	95,86	0,54	0,01	15,61	4,16	0,72	36,30	50,50	9,10	4,60		
T2-21	tuffite		9,23	0,83	2,04	1,81	352,85	1,03	2,41	178,16	0,50	0,04	9,53	7,26	0,778	33,40	42,90	7,60	3,20		
T2-22	547533	2574875	8,58	0,83	1,99	1,81	376,54	0,88	2,41	166,07	0,44	0,07	7,63	14,20	0,757	32,30	42,70	8,10	3,50		
T2-23	Fara Fm.	Autochthon A	12,48	0,83	2,32	1,81	377,81	1,01	2,41	163,95	0,43	0,03	11,07	5,44	0,789	40,20	51,00	7,30	3,70		
T2-24			6,16	0,83	1,26	1,81	186,92	0,52	2,41	76,65	0,41	0,03	10,98	4,83	0,768	36,80	48,00	7,80	3,80		
T3-21	sandstone		3,69	0,86	1,04	1,81	361,71	0,41	2,41	142,73	0,39	0,02	15,90	6,29	0,689	26,90	39,10	10,00	3,90		
T3-22	544722	2570255	2,82	0,88	0,63	1,82	254,57	0,22	2,42	87,47	0,34	0,02	12,85	9,07	0,694	34,20	49,40	9,90	4,90		
T3-23	Muaydin Fm.	Autochthon A	1,54	0,90	0,35	1,85	116,01	0,23	2,42	75,70	0,65	0,02	17,64	5,19	0,67	31,80	47,50	10,50	5,00		
T3-24			4,71	0,84	1,20	1,81	309,13	0,70	2,41	180,18	0,58	0,05	9,18	12,12	0,74	28,50	38,50	8,60	3,30	42,60 +/- 1,70	
T3-25			8,91	0,83	1,95	1,81	262,57	1,30	2,41	175,08	0,67	0,07	9,00	9,29	0,761	32,60	42,90	8,00	3,40		
T3-26			9,80	0,83	2,52	1,81	283,31	1,13	2,41	127,16	0,45	0,06	7,80	6,56	0,816	29,00	35,60	6,60	2,30		
T3-27			11,83	0,83	2,41	1,81	219,27	1,23	2,41	111,66	0,51	0,11	7,31	10,01	0,794	36,10	45,50	7,10	3,20		
T3-28			8,41	0,83	1,85	1,81	224,86	1,04	2,41	125,92	0,56	0,07	9,09	8,40	0,784	33,10	42,20	7,40	3,10		
T4-21	conglomerate		18,23	0,83	1,79	1,81	380,98	0,44	2,41	93,57	0,25	0,02	13,79	3,77	0,736	79,30	107,60	8,70	9,40		
T4-22	517510	2560808	10,68	0,83	1,36	1,81	392,55	0,35	2,41	100,65	0,26	0,02	15,99	5,30	0,703	61,20	86,90	9,60	8,40	93,80 +/- 6,90	
T4-23	Muti Fm.	Autochthon B	5,24	0,85	0,56	1,82	137,78	0,48	2,41	118,23	0,86	0,04	8,48	11,06	0,738	64,20	86,90	8,60	7,50		
T5-21	turbiditic sandstone		34,15	0,82	3,38	1,81	502,17	0,79	2,41	117,95	0,23	0,10	7,97	14,16	0,781	78,70	100,80	7,50	7,60	106,00 +/- 5,20	
T5-22	512934	2561691	13,52	0,83	1,28	1,81	333,42	0,27	2,41	69,42	0,21	0,02	16,57	4,11	0,744	82,70	111,20	8,50	9,50		
T5-23	Matbat Fm.	Hasawina N.	8,95	0,83	1,30	1,81	254,43	0,78	2,41	153,35	0,60	0,01	16,47	2,78	0,754	49,70	65,90	8,20	5,40	58,90 +/- 7,00	
T5-24			9,21	0,84	1,75	1,81	416,93	0,69	2,41	163,29	0,39	0,04	9,44	9,25	0,766	39,80	51,90	7,90	4,10		
T5-25			37,88	0,80	51,13	2,33	1,81	561,72	0,37	2,41	90,14	0,16	0,02	11,59	0,741	128,10	172,90	8,60	14,90		
T6-21	granodiorite		6,55	0,83	1,00	1,81	241,80	1,28	2,41	311,91	1,29	0,29	5,62	69,36	0,747	41,60	55,60	8,30	4,60		
T6-22	478301	2592360	6,39	0,85	0,97	1,81	288,96	1,32	2,41	394,16	1,36	0,28	5,31	84,38	0,719	41,10	57,20	9,10	5,20		
T6-23	Trondjemite	Semail Ophio.	7,07	0,83	1,06	1,81	314,75	1,79	2,41	528,55	1,68	0,19	5,49	57,19	0,751	39,20	52,30	8,20	4,30	53,70 +/- 1,20	
T6-24			12,11	0,84	1,79	1,81	347,26	1,35	2,41	649,55	1,87	0,31	5,55	61,00	0,769	38,60	50,20	7,70	3,80		
T6-25			6,78	0,84	1,08	1,81	273,36	1,46	2,41	368,85	1,35	0,27	5,75	68,70	0,738	39,10	53,00	8,60	4,50		
T7-21	quartzite		14,91	0,84	1,56	1,81	427,30	0,43	2,41	118,20	0,28	0,05	9,26	12,45	0,744	73,80	99,20	8,50	8,50	99,20	
T7-22	514817	2586049	4,14	0,87	1,35	1,81	428,75	0,38	2,41	119,50	0,28	0,02	12,47	7,90	0,729	23,70	32,50	8,90	2,90		
T7-23	Matbat Fm.	Hasawina N.	6,37	0,85	1,33	1,81	274,36	0,30	2,41	62,67	0,23	0,03	10,62	6,71	0,769	37,50	48,80	7,90	3,80	43,00 +/- 3,70	
T7-24			9,66	0,81	12,43	2,13	1,81	539,06	0,15	2,41	38,38	0,07	0,01	17,24	0,777	36,90	47,50	7,70	3,70		
T7-25			4,03	0,83	5,46	0,94	1,81	232,12	0,47	2,41	115,05	0,50	0,02	12,63	0,738	31,70	43,00	8,60	3,70		
T8-21	tuffitic sandstone		4,60	0,86	1,34	1,81	450,89	1,11	2,41	374,66	0,83	0,16	5,81	53,52	0,759	23,70	31,20	8,00	2,50		
T8-22	532600	2578681	2,92	0,85	0,56	1,82	147,09	0,86	2,41	226,75	1,54	0,28	5,14	73,06	0,715	31,40	44,00	9,20	4,00	39,80 +/- 3,00	
T8-23	Mistal Fm.	Autochthon A	2,21	0,89	0,46	1,83	168,48	0,57	2,41	208,48	1,24	0,05	8,65	16,66	0,716	30,90	43,20	9,20	4,00		
T8-24			3,46	0,85	0,85	1,81	212,57	0,41	2,41	103,10	0,49	0,01	14,27	3,65	0,74	30,30	41,00	8,60	3,50		
T9-21	quartzite		2,90	0,86	0,61	1,82	238,35	0,50	2,41	198,12	0,83	0,01	16,09	5,23	0,705	33,10	46,90	9,50	4,50		
T9-22	532595	2568258	0,72	0,98	0,18	1,94	109,52	0,13	2,43	76,58	0,70	0,05	10,52	29,38	0,674	27,50	40,80	10,50	4,30	45,50 +/- 2,40	
T9-23	Mistal Fm.	Autochthon A	2,04	0,89	0,41	1,84	147,39	0,28	2,41	101,51	0,69	0,01	18,70	3,60	0,718	35,10	48,80	9,20	4,50		
T10-21	sandstone		5,09	0,85	0,93	1,81	213,39	0,95	2,41	217,83	1,02	0,02	13,41	4,93	0,754	36,40	48,20	8,10	3,90		
T10-22	534779	2572636	6,71	0,83	1,37	1,81	267,61	1,24	2,41	241,07	0,90	0,04	9,18	8,32	0,763	33,30	43,70	7,90	3,40	46,90 +/- 4,10	
T10-23	Mistal Fm.	Autochthon A	8,97	0,83	2,25	1,81	568,33	1,79	2,41	452,52	0,80	0,04	8,74	10,22	0,723	27,70	38,40	9,00	3,50		
T10-24			2,26	0,88	0,35	1,85	118,10	0,39	2,41	131,18	1,11	0,02	14,08	5,39	0,727	41,80	57,50	8,90	5,10		
T11-21	quartzite		4,70	0,84	1,01	1,81	188,02	0,57	2,41	106,02	0,56	0,01	19,39	2,18	0,746	34,00	45,60	8,40	3,80		
T11-22	540394	2572230	1,55	0,90	0,39	1,84	109,55	0,31	2,41	93,99	0,86	0,01	20,85	2,31	0,706	27,30	38,80	17,60	6,80	42,50 +/- 2,00	
T11-23	Mistal Fm.	Autochthon A	1,50	0,94	0,37	1,84	110,19	0,19	2,42	56,69	0,51	0,01	17,25	3,39	0,693	29,90	43,20	9,90	4,30		
T12-21	sandstone		5,35	0,85	1,21	1,81	355,93	1,09	2,41	320,43	0,90	0,02	16,47	5,58	0,706	30,10	42,70	9,50	4,00		
T12-22	531776	2582871	4,28	0,86	1,12	1,81	286,68	0,16	2,42	40,59	0,14	0,01	27,93	1,79	0,736	30,70	41,70	8,80	3,70	40,10 +/- 1,50	
T12-23	Sahtan Gp.	Autoch																			

351 **Table 2: Results of zircon (U-Th)/He dating.**

352



353

354 **Figure 4:** Map view of ZHe ages sampled below, in and above the carbonate platform of the Jebel Akhdar Dome. Data
355 outlines a general cooling between 58.9 ± 7.0 and 39.8 ± 3.0 Ma. Some samples outside of the dome show two age
356 populations, with an additional age population of c. 100 Ma. Additional temperature data refers to zircon fission track
357 ages of (*) Saddiqi et al. (2006), Apatite fission track ages of (Δ) Poupeau et al. (1998) and (+) Mount et al. (1998), and
358 AHe, AFT and ZFT ages of (+, grey) Hansmann et al. (2017). Moreover, the locations of samples (see) for fluid inclusion
359 measurements are shown. Colors in the background depict geological units as defined in Figure

360 These ages indicate a large-scale cooling signal that affects the study area and is associated with doming.
361 The ZHe age pattern and 1D thermal models (Figures S3 and S4) indicate a phase of rapid cooling below 170 °C
362 in the early Cenozoic (58.9 ± 7.0 to 39.8 ± 3.0 Ma). The range of modeled cooling paths outline minimum and
363 maximum cooling rates of 2-8 °C/M.yr. This is followed by slower cooling until the present day.

364 Data from the Muti Fm. and the Hawasina units differ partly from the trend: the apparent ZHe age of the Muti
365 sample T4 (93.8 ± 6.9 Ma) is as old as its respective stratigraphic age (Turonian-Campanian; Robertson, 1987)
366 indicating only partial reset of the ZHe system. Samples of the lower Hawasina Nappes contain two grain age
367 populations. Older ages coincide with higher uranium concentrations (sub) suggesting that only the younger ages
368 represent thermally reset zircons. The older ZHe population of 110-95 Ma coincides with timing of forebulge
369 migration through the area, as independently determined in the stratigraphic record in the Wasia-Aruma Break
370 (Figure 3). Partial reset of ZHe ages suggests that the Hawasina samples have not experienced temperatures
371 exceeding the partial retention zone (PRZ) of 150-170 °C.

372 A magmatic sample of an intrusive from the Semail Ophiolite yields ZHe ages of 53.7 ± 1.2 Ma (T6) with a
373 modeled cooling path gradually decreasing into the PRZ until c. 55 Ma. This time interval of passing the PRZ is
374 comparable to the Hawasina nappe samples beneath the ophiolite but occurs slightly earlier than cooling of the
375 Autochthonous. Nevertheless, Semail Ophiolite, Hawasina Nappes and the autochthonous margin sequence were
376 affected by the same cooling event that was possibly initiated by exhumation of the Jebel Akhdar Dome.

377 **4.3. Fluid inclusions**

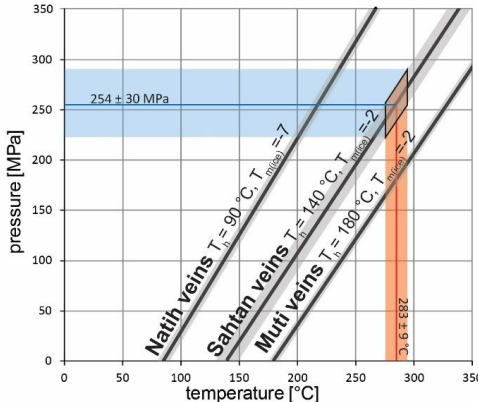
378 The Muti veins' samples FI-M1 and M2 of the southern Jebel Akhdar s evidence of crack and seal processes
 379 (youngest parts in the center of the vein, Ma-2010-11b and 14a of [Al-Natih 2015](#)) with blocky quartz grains that
 380 contain two kinds of roundish primary FIs with sizes of 3-20 μm . They are mainly aligned along dark zones and
 381 are interpreted as growth zones or form bright clusters in the central part of the crystals. A third set of fluid
 382 inclusions (FIs) appears in large, grain-crosscutting trails interpreted to be of secondary origin. Calcite crystals
 383 within the Natih veins contain bright FIs with sizes of 2-20 μm and are edgy, often rectangular or trapezoidal in
 384 shape. Identified primary FIs are aligned parallel to crystal growth zones.
 385 All measured FIs are two-phase, liquid-vapor inclusions with ice as last phase to melt. The Muti samples show
 386 $T_{\text{fm(ice)}}$ between -5.1 ± 0.5 and -4.6 ± 0.3 $^{\circ}\text{C}$ and $T_{\text{m(ice)}}$ at -2.2 ± 0.2 to -1.9 ± 0.1 $^{\circ}\text{C}$, the Natih sample T_{fm} of $-$
 387 18.4 ± 1.9 to -20.2 ± 2.1 $^{\circ}\text{C}$ and $T_{\text{m(ice)}}$ of -7.1 ± 0.3 to -8.9 ± 1.8 $^{\circ}\text{C}$ (Table 3). First melting temperatures of all
 388 inclusions correspond to an $\text{H}_2\text{O}-\text{NaCl}$ system and complete melting temperatures of ice indicate salinities similar
 389 to seawater (3.0 ± 0.5 to 3.5 ± 0.3 wt.-% NaCl eq., Muti Fm.) or three times higher (10.3 ± 0.3 to 12.5 ± 2.0 wt.-%
 390 NaCl eq., Natih Fm.).
 391

392 **Table 3: Results of FI thermometry.** Identified FI types, their measured homogenization temperatures and results of
 393 the pressure correction for 280 and 340 MPa accounting for 8 and 10 km of ophiolite with partly serpentinized mantle
 394 sequence and 2 km of sedimentary nappes, and for 45 MPa accounting for 2 km of sedimentary overburden for samples
 395 unaffected by ophiolite obduction. First melting (T_{fm}) and final melting of ice ($T_{\text{m(ice)}}$) temperatures and salinities are
 396 given. Data of Holland et al. (2009) is added for comparison and we likewise corrected his homogenization temperatures
 397 for pressures of 280 and 340 MPa, as his samples were originally covered by the ophiolite complex. (* further heating
 398 was avoided to prevent inclusion damage)

sample No.	vein orient., location and host mineral	FI kind	No. of FIA	T_{hom} [$^{\circ}\text{C}$]	pressure corrected T [$^{\circ}\text{C}$] for 45 MPa	T_{fm} [$^{\circ}\text{C}$]	$T_{\text{m(ice)}}$ [$^{\circ}\text{C}$]	salinity [wt.-% NaCl]
FI-M1	NE-SW striking	primary	21	$166 \pm/- 7$	$189 \pm/- 7$	$-4.7 \pm/- 0.2$	$-2.2 \pm/- 0.2$	$3.5 \pm/- 0.3$
	strike-slip vein (IX), Muti Fm.	primary	22	$189 \pm/- 3$	$213 \pm/- 3$	$-4.6 \pm/- 0.3$	$-2.0 \pm/- 0.3$	$3.2 \pm/- 0.4$
	Gorge area, quartz	secondary	18	$> 200^*$	> 224	$-4.6 \pm/- 0.2$	$-2.0 \pm/- 0$	$3.2 \pm/- 0$
pressure corrected T [$^{\circ}\text{C}$] for 45 MPa								
FI-M2	NE-SW striking	primary	24	$161 \pm/- 3$	$184 \pm/- 3$	$-5.1 \pm/- 0.5$	$-1.9 \pm/- 0.1$	$3.0 \pm/- 0.2$
	strike-slip vein (IX), Muti Fm.	secondary	12	$116 \pm/- 12$	$138 \pm/- 12$	-	-	-
	Gorge area, quartz	secondary	24	$150 \pm/- 2$	$172 \pm/- 2$	-	-	-
for 280 MPa for 340 MPa								
FI-N1	Natih Fm., NW-SE	primary	14	$90 \pm/- 5$	$235 \pm/- 5$	$266 \pm/- 5$	$-18.4 \pm/- 1.9$	$-7.1 \pm/- 0.3$
	burial vein (III), Wadi Nakhr, calcite	primary	26	$(114 \pm/- 7)$	$(264 \pm/- 7)$	$(297 \pm/- 7)$	$-20.2 \pm/- 2.1$	$-8.9 \pm/- 1.8$
for 280 MPa for 340 MPa								
FI-N2	Natih Fm., early E-W vein (I)	primary	10	$80 \pm/- 4$	$225 \pm/- 4$	$256 \pm/- 4$	-	-
	Al Raheba, calcite							
for 280 MPa for 340 MPa								
399	Holland et al. (2009)	Sahtan Gp., bedding parallel shear vein, top-to-NE (IV), Wadi Nakhr, quartz	primary and pseudosec.	n.a.	134-141	296-303	357-364	from -19 -3.7 to -2.3 3.8 to 6.0
400								



401 Primary inclusions in quartz crystals from the Muti Fm. show minimum trapping temperatures of 161 ± 3 to
402 166 ± 7 °C (Table 3, FI-M2 and middle of FI-M1) with a second primary population of 189 ± 3 °C (sides of vein
403 FI-M1). T_h of secondary inclusions in FI-M1 are above 200 °C. In sample FI-M2, two generations of secondary
404 inclusions were observed, both reflecting lower T_h than the primary inclusions. No hints of necking down, leakage
405 or stretching were observed at the measured inclusions and over 90 % of the measured FIs in one assemblage are
406 in the range of 10-15 °C representing a good quality of the measurements (Goldstein, 2001).
407 Samples FI-N1 and N2 of the Natih Fm. in the southern Jebel Akhdar (Figure 4) contain primary inclusions hosted
408 by calcite crystals giving T_h of 80 ± 4 , 90 ± 5 and 114 ± 7 °C (Table 3). The latter population is often characterized
409 by elongated, possibly stretched FI, and is not considered for further interpretations. Assuming vein formation
410 during burial (Grobe et al., 2018; Hilgers et al., 2006; Holland et al., 2009; Virgo, 2015) under 8 to 10 km of
411 ophiolite including partially serpentinized peridotite and 2 km of Hawasina Nappes, results were pressure
412 corrected for 280 and 340 MPa leading to corrected homogenization temperatures of 235 ± 5 and 266 ± 5 °C (FI-
413 N1), and 225 ± 4 and 256 ± 4 °C (FI-N2, Table 3). Signs of strong deformation such as twinning or cleavage were
414 not observed in the measured inclusions; secondary inclusions were present but not measured.
415 These temperatures represent minimum trapping conditions of a paleo-fluid and do not necessarily represent burial
416 temperatures of the host rock. It should be noted that the analyzed Natih veins formed bedding confined (Grobe et
417 al., 2018; Holland et al., 2009; Virgo, 2015) and show host rock buffered carbonate isotope signatures (Arndt et
418 al., 2014; Hilgers et al., 2006). This corroborates the idea that analyzed veins were in thermal equilibrium with
419 their host rocks.
420 FI thermometry of late strike-slip veins in the Muti Fm. are interpreted to have formed after dome formation (Grobe
421 et al., 2018; Virgo, 2015) at an assumed depth of 2 km. A pressure correction for the related 45 MPa corresponds
422 to minimum fluid trapping temperatures of 184 ± 3 °C (FI-M2) and 213 ± 3 °C (FI-M1) with a later phase of
423 primary inclusions outlining 189 ± 7 °C and even cooler secondary inclusions of 138 ± 12 to 172 ± 2 °C (FI-M1
424 and M2, Table 3). These cooler fluid temperatures can be explained by further exhumation of the Jebel Akhdar
425 and, hence, cooling of the fluids' reservoir during crack-seal vein formation. Isotope studies on the vein calcite do
426 not support an open system with fluid exchange (Stenhouse, 2014; Virgo and Arndt, 2010), hence, we interpret
427 the formation of strike-slip related veins as having formed during exhumation following peak burial.
428 Based on the assumption that fluid and host rock were in thermal equilibrium, we can use maturity data in
429 combination with fluid inclusion data to estimate the pressure at vein formation. Peak temperatures of the Sahtan
430 Fm. revealed by RSCM reached 283 ± 9 to 286 ± 6 °C (Table 1, Figure 5 red line) and enable to solve the pressure-
431 temperature couples of FIs measured in Sahtan veins formed at deepest burial by Holland et al. (2009, black line).
432 This results in minimum trapping pressures of 254 ± 30 MPa at times of vein formation (Figure 5 blue line), which
433 correspond to times close to or at deepest burial of the carbonate platform.



434
 435
 436
 437
 438
 439

Figure 5: Fluid inclusion isochores (solid black lines) of analyzed fluid inclusion populations with corresponding std. deviations (shaded areas, for Sahtan Gp. data of Holland et al., 2009, conservatively $\pm 10^\circ\text{C}$ are assumed). To estimate the pressure conditions during vein formation, calculated temperatures from thermal maturity data are added for the Sahtan Gp. (red line with error) and result in minimum trapping pressures of 254 ± 30 MPa during peak burial (blue line with error).

440

4.4. Structural observations



441
 442
 443
 444
 445
 446
 447

The reconstructed transect (Figure 2) shows the dome structure of the Jebel Akhdar covered with ophiolite nappe remnants in the northeast, the thrusted southern foreland and the salt basins in the southeast that contain the fault-bound hydrocarbon reservoirs of the Fahud and Natih fields. Structures shown are related to large scale normal faulting in the mountain area, where faults are subsequently rotated and bent by doming (Jebel Akhdar), and later strike-slip faulting crosscut domed layers (Gomez-Rivas et al., 2014; Grobe et al., 2018; Virgo, 2015). Reactivation and inversion of some of the strike-slip faults caused formation of hydrocarbon traps in the southern foreland (Natih and Fahud field, e.g. Al-Kindi and Richard, 2014).

448

4.5. Basin modeling

449
 450
 451
 452
 453

Numerical basin modeling integrates all data and tests the individual interpretations in the thermal and geodynamic framework. Deepest burial was constrained with thermal maturity data and exhumation with thermochronological data. In the following we present our best fit model, considering a mixed ophiolite lithology (Searle and Cox, 2002) consisting of strongly serpentinized peridotites. Then, the sensitivity of important results to changes of relevant input parameters are discussed.

454
 455
 456
 457
 458
 459
 460

Modeled evolution of the transect over time is given in Figures 8–9, showing (a) final deposition of the Autochthonous B, (b) erosion of the Natih Fm. in the North by a moving foredeep, (c) emplacement of Hawasina Nappes, and d–e) ophiolite obduction reconstructed by rapid, stepwise sedimentation. After maximum burial beneath the ophiolite complex at c. 80 Ma (Warren et al., 2005) exhumation is assumed to start slightly prior to 55 Ma (Saddiqi et al., 2006) with a rapid phase of cooling below c. 200°C at 55 Ma leading to lower temperatures in the Jebel Akhdar region. 1D burial plots of two pseudo-wells created out of point data in Wadi Nakhr and Wadi Yiqah are shown in the electronic supplement Figure S5.

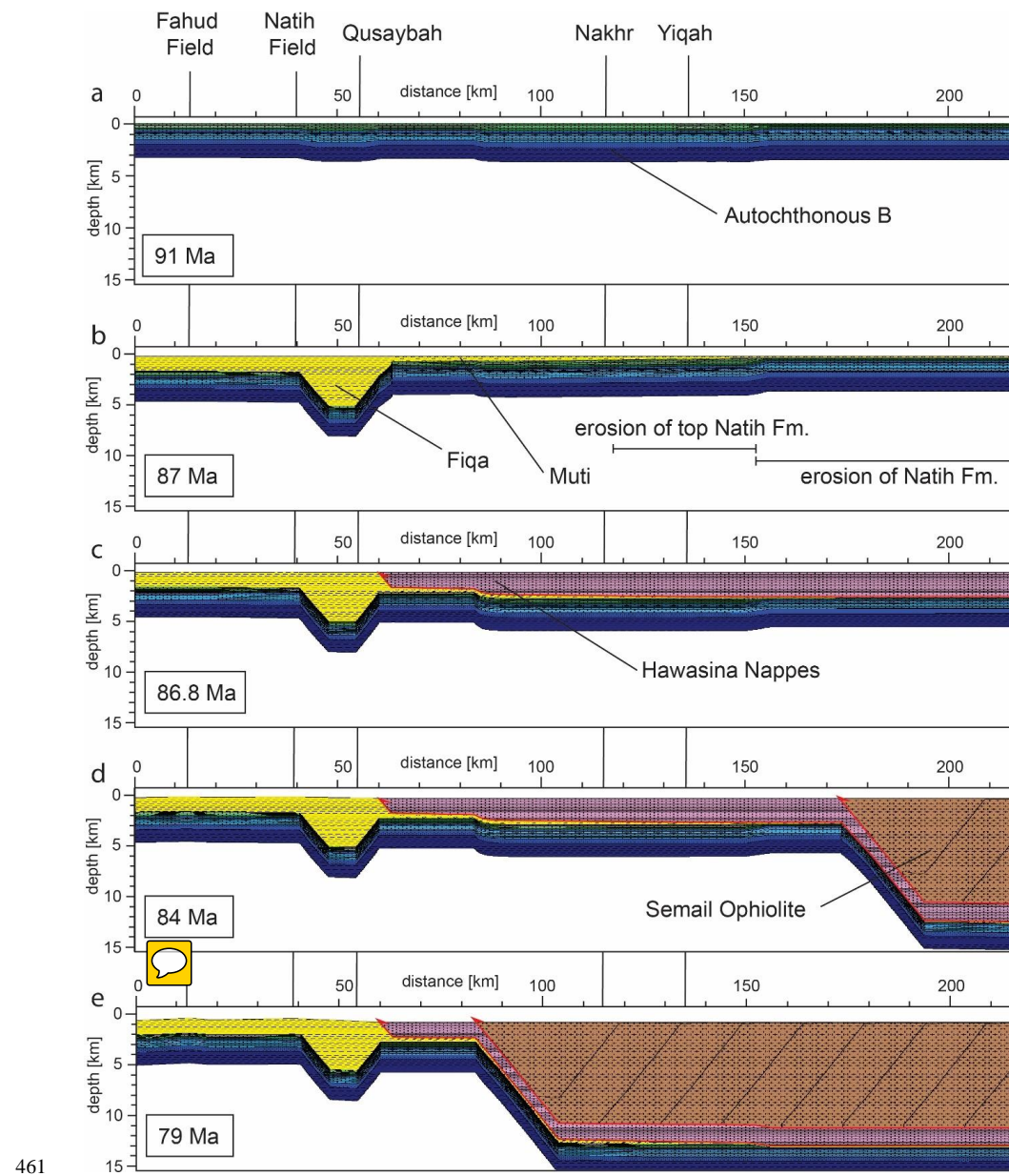
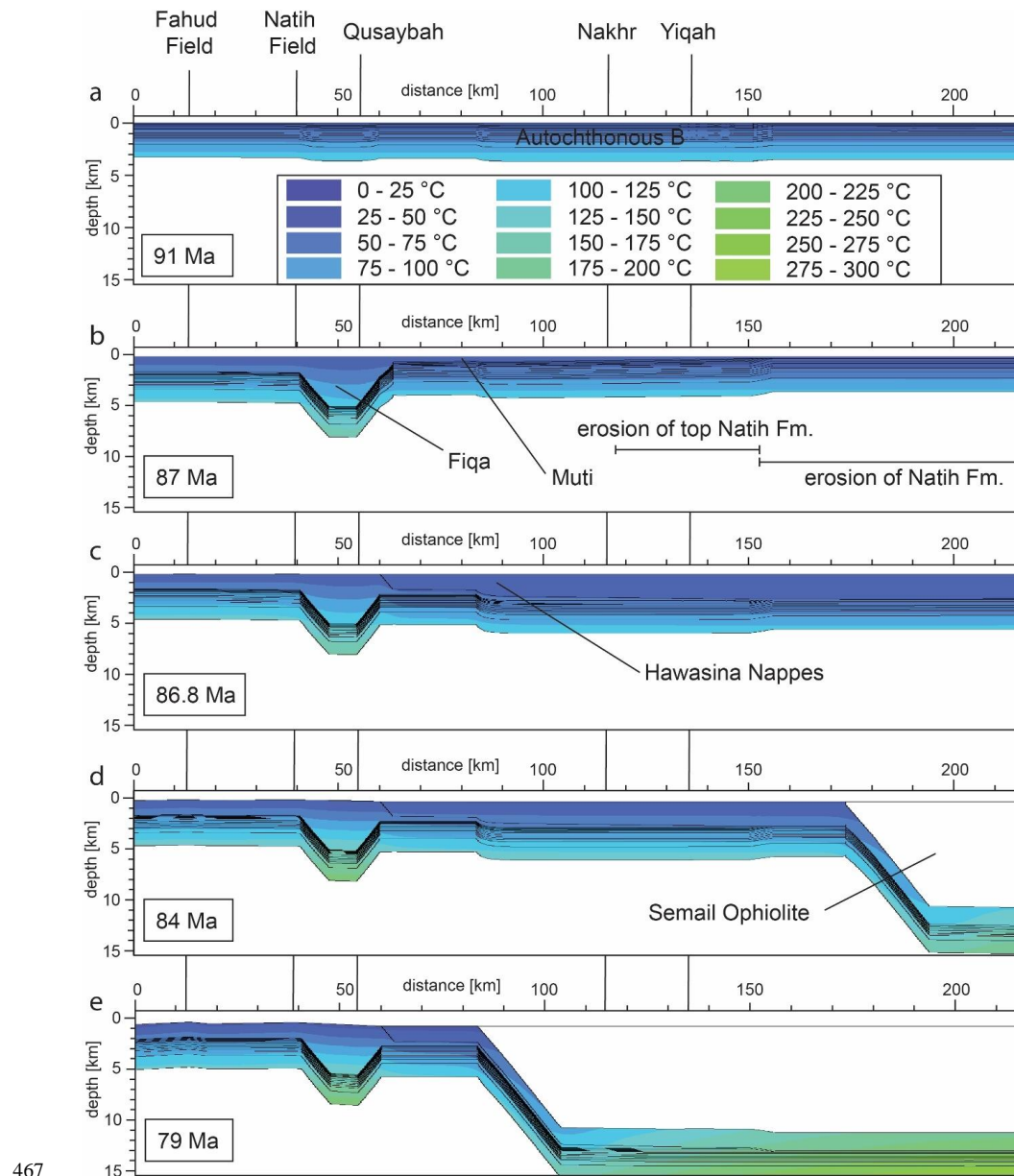


Figure 6: Modeling results: Transect evolution from sedimentation of the Autochthonous B at stable passive margin conditions (a), to moving foredeep that finally filled with Fiqa sediments (b, peak burial as calibrated by thermal maturity data), Hawasina Nappe (c) and ophiolite emplacement (d) leading to deepest basin (e). Highlighted with vertical lines in the background are the locations of present-day oil fields and sampling site.



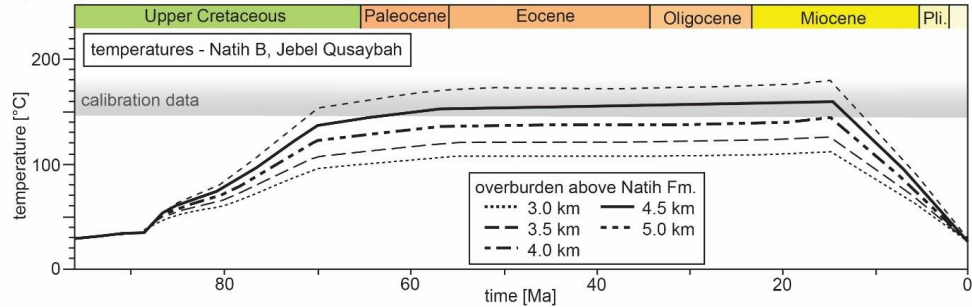
467
468
469 **Figure 7: Modeling results: Temperature evolution of the transect of Figure 6. Highlighted with vertical lines in the**
470 **background are the locations of present-day oil fields and sampling sites.**

471
472 As a model set up only presents one possible solution out of several, sensitivity analyses with varying paleo-
473 overburden thicknesses (Figures 8 and 9), changing degree of serpentization of the ophiolite and varying basal
474 heat flow during deepest burial (Figure 10) are presented and discussed below.

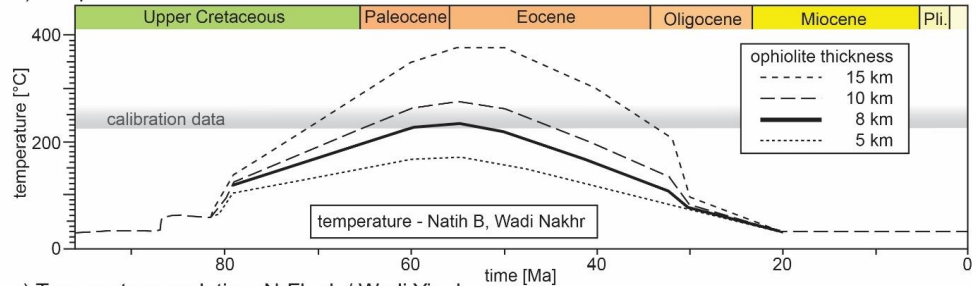


475 Thermal maturity data of the Natih B at Jebel Qusaybah (1.1-1.8 % VR_t), Adam Foothills, requires peak
476 temperatures of 145-182 °C (Table 1). Sensitivity analyzes of the overburden above the Natih Fm. outlined that at
477 least 4 to 4.5 km of sedimentary overburden (Figures 8a and 9a) are needed to match the calibration data.
478

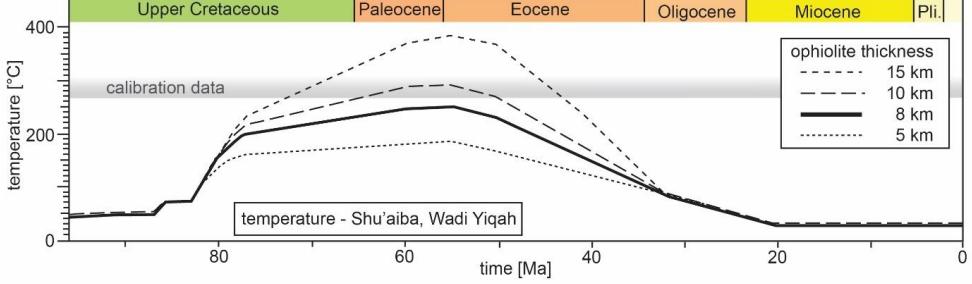
a) Temperature evolution: Foredeep / Jebel Qusaybah



b) Temperature evolution: S-Flank / Wadi Nakhr



c) Temperature evolution: N-Flank / Wadi Yiqah

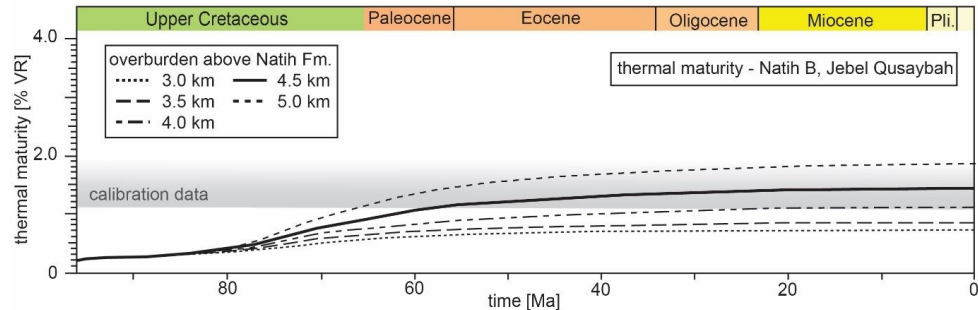


479

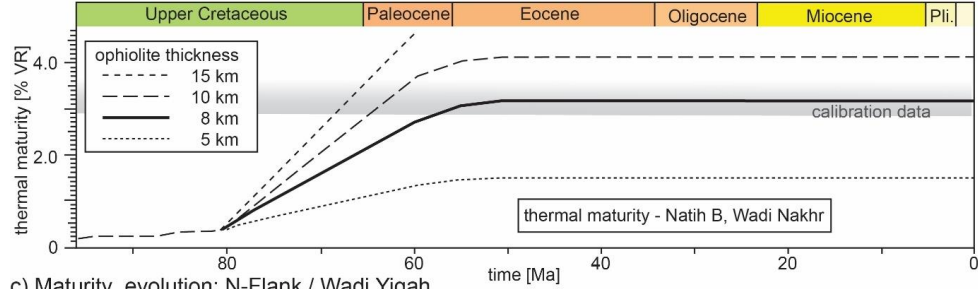
480 **Figure 8: Sensitivity analysis of paleo-overburden and its influences on temperature in comparison to calculated peak**
481 **temperatures (gray area) for pseudo-wells at Jebel Qusaybah (a), Wadi Nakhr (b) and Wadi Yiqah (c).**



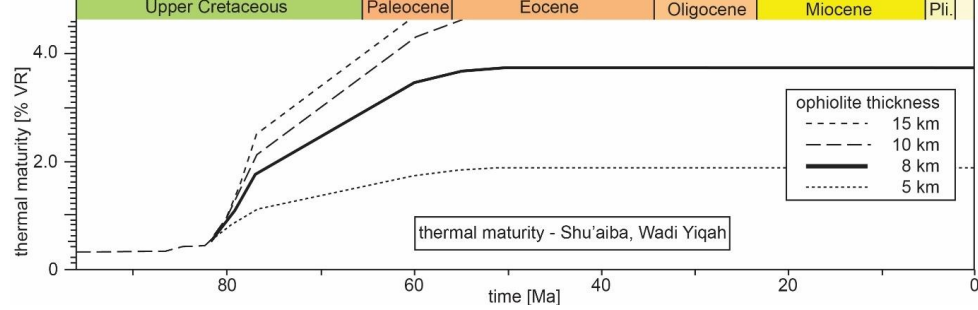
a) Maturity calibration: Foredeep / Jebel Qusaybah



b) Maturity calibration: S-Flank / Wadi Nakhr



c) Maturity evolution: N-Flank / Wadi Yiqah



482

483

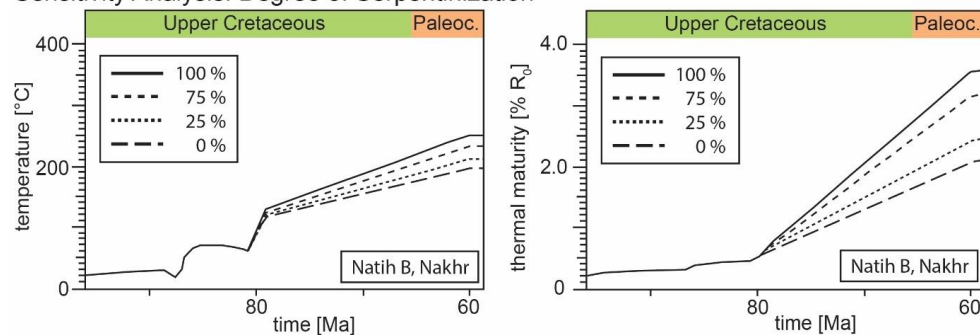
484 **Figure 9: Sensitivity analysis of paleo-overburden and its influences on thermal maturity in comparison to calibration**
 485 **data (gray area). Data is used to calibrate burial depth of the foredeep at the Jebel Qusaybah (a), paleo-ophiolite**
 486 **thickness at the southern flank of the Mountains at Nakhr (b) and at its northern counterpart at Yiqah (c).**

487 To restore the former thickness of the Semail Ophiolite the thickness of the Hawasina Nappes along the transect
 488 was fixed to 2 km, representing its minimum thickness as suggested by the maximum present-day thickness of the
 489 Jebel Misht exotics. To reach required thermal conditions measured at the entrance of the Wadi Nakhr (Natih B: 2.83-3.72 % VR_r, 225-260 °C; Grobe et al. 2016), 8-10 km of original, total thickness of strongly serpentinized
 490 ophiolite sequence are needed in addition to the assumed 2 km of Hawasina Nappes (Figures 8b and 9b). These
 491 thicknesses are also sufficient to reach peak temperatures calculated for older stratigraphy at the northern flank of
 492 the Jebel Akhdar Dome (Shu'aiba Fm. at Wadi Yiqah: 270-295 °C by RSCM, Figures 8c and 9c). Modeling results
 493 show a longer-lasting,  increase in maturity and temperature in the north, which we interpret as associated
 494 with the 2 Mys earlier onset of obduction and, hence, a longer burial of the northern carbonate platform (Wadi
 495 Yiqah) under the active ophiolite obduction compared to its southern counterpart (Wadi Nakhr; Béchennec et al.,
 496 1990; Cowan et al., 2014).

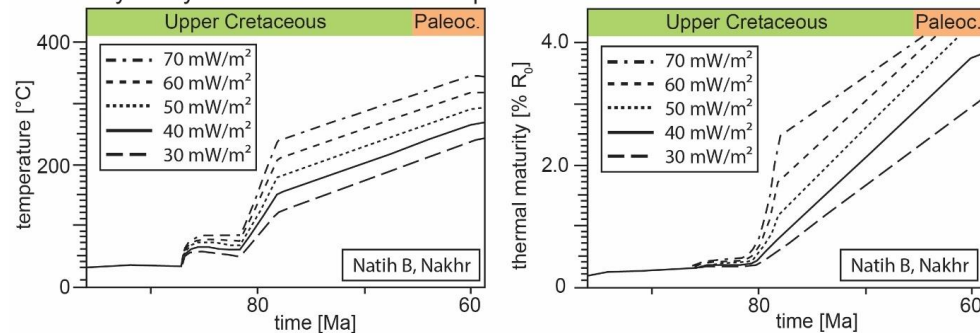


498 Another factor influencing the modeling results is related to the lithology of the overburden and its compaction.
 499 In the special case of burial under an ophiolite, serpentinization of peridotite and its impact on ophiolite density
 500 and thermal conductivity must be considered. Sensitivity analysis of ophiolite serpentinization shows the
 501 temperature and thermal maturity effects on our model (Figure 10). A model-case of ophiolite without any
 502 serpentinized peridotite (0 %-case, $\rho_{\text{ophio}}=3133 \text{ kg/m}^3$) would represent the largest deviation compared to our best-
 503 case model assuming complete ophiolite serpentinization (100 %-case, $\rho_{\text{ophio}}=3069 \text{ kg/m}^3$). This density is based
 504 on Al-Lazki et al. (2002). Even if the upper part of the ophiolite is missing in the Jebel Akhdar area, this and the
 505 observations of Searle and Cox (2002) in the Saih Hatat support strong serpentinization. A less serpentinized
 506 ophiolite means higher densities and related higher thermal conductivities of the overburden and thus lower peak
 507 temperatures in the sediments below. In a no-serpentinization case, peak temperature of Natih B in the Wadi Nakhr
 508 would decrease by c. 60 °C resulting in a maximum thermal maturity decrease of 1.5 % VR. The best fit model
 509 with an ophiolite thickness of 8-10 km would need additional 3 km of overburden at 0 % serpentinization to
 510 equally match the measured thermal maturities. Additional thicknesses of 0.75 km (75 % serpentinization), 1.5 km
 511 (50 % serpentinization) and 2.25 km (25 % serpentinization) apply for lower degrees of serpentinization,
 512 respectively.
 513 Results depend strongly on basal heat flow (Figure S2). The best fit model of 40 mW/m² at deepest burial is typical
 514 for a passive continental margin setting. If this heat flow at peak burial would be lowered to 30 mW/m² an
 515 additional amount of 1.2 km of ophiolitic overburden would be required to achieve a match with thermal
 516 calibration data (Figure 10). Increased heat flow values to 50, 60 or 70 mW/m² would result in less overburden of
 517 -1.3, -2.4 and -3.5 km, respectively (Figure 10).
 518

Sensitivity Analysis: Degree of Serpentinization



Sensitivity Analysis: Heatflow variation at peak burial



519



520 **Figure 10: Sensitivity analysis: Top: Different degrees of serpentinization of the peridotite within the Semail Ophiolite**
521 **affect the temperature (left) and thermal maturity (right) evolution (modeled for Natih B Fm. at Wadi Nakhr). Pure**
522 **peridotite (0 % serpentinization) require additional 3 km of ophiolite in addition to the 8-10 km of the best-fit model to**
523 **equally match the calibration data. 100 % refers to complete serpentinization of the peridotite in the ophiolite. Bottom:**
524 **The influence of variable heat flow values at peak burial on temperature (left) and thermal maturity (right).**

525 **5. Discussion**

526 Any basin and petroleum system model has to deal with uncertainties, in particular for complex areas such as the
527 Jebel Akhdar, where sedimentary rocks reached high temperatures and maturities due to deep and rapid burial. In
528 the following, we discuss these uncertainties with respect to temperature and burial history, overpressure build-up
529 and induced fluid flow. For all presented basin models of the study area, the following limitations apply: (1)
530 decompacting the present-day lithologies does not consider rock volume lost by pressure solution. This is probably
531 of minor importance in our study area as host-rock buffered isotope ratios of the veins were interpreted as local
532 sinks for nearby dissolved calcite (Arndt et al., 2014; Hilgers et al., 2006), so that the overall rock volume remains
533 approximately constant, (2) decompaction only accounts for burial, whereas a possible tectonic compaction is
534 neglected (Neumaier, 2015) and (3) calculated overpressure does not include a rock volume decrease due to
535 pressure solution.

536 **5.1. Burial history**

537 Little is known about the very early phase of burial, before 91 Ma (Figures 6 and 7, Grobe et al., 2018). The
538 assumptions for this period are based on hypotheses on the tectonic evolution of the passive continental margin as
539 well as data on thickness of sedimentary units but are not strongly constrained by petrographic data.

540 In Turonian times (93.9-89.6 Ma; Robertson, 1987) a southwest-ward-moving forebulge, related to plate
541 convergence, affected northern Oman. It eroded the northeastern platform edge and migrated southwest-ward to
542 the present-day position of the Adam Foothills (Robertson, 1987). Measured thermal maturities of 1.1-1.8 % VR,
543 were used to reconstruct peak temperatures during burial in Jebel Qusaybah, Adam Foothills, which range between
544 145 and 182 °C. Numerical basin modeling results reveal that additional paleo-overburden of at least 4 to 4.5 km
545 (Natih B, Qusaybah,

546 Figure 9) is required to reach these temperatures. The exhumation history of the Adam Foothills is not well known;
547 our model is based on an interpreted late exhumation during the Miocene (Claringbould et al., 2013). Earlier
548 exhumation would shorten the time span of the rock at higher temperatures (Figure 7), lead to decreased thermal
549 maturity and, hence, would require additional overburden to match the measured thermal maturity data. Therefore,
550 the resulting burial of 4 to 4.5 km has to be regarded as minimum value, which would increase by pre-Miocene
551 exhumation of the Jebel Qusaybah. South of the Adam Foothills basin geometries are not affected by the moving
552 foredeep. Here peak burial was reached under c. 3 km of Fiqa, Hadhramaut and Fars formations. This is based on
553 the assumption that present-day burial equals deepest burial as no thermal calibration data of the area south of
554 Jebel Qusaybah was achieved, which is in agreement with interpretations of Terken (1999) and Warburton et al.
555 (1990).

556 In case of the Jebel Akhdar, peak temperatures were reached as a consequence of burial below the ophiolite (e.g.
557 Loosveld et al., 1996; Searle, 2007; Searle et al., 2003; Warren et al., 2005). Here the sedimentary rocks reached
558 high temperatures and maturities as shown by solid bitumen reflectance, RSCM, FT-IR and Rock-Eval pyrolysis
559 data (Table 1; Fink et al., 2015; Grobe et al., 2016). Pre-obduction burial by sedimentation is not sufficient for



560 such high thermal maturities, and it likewise cannot be explained by increased basal heat flow before 91 Ma or
561 after 55 Ma. Influence of local hydrothermal effects cannot be excluded, but because the entire Jebel Akhdar
562 reached high temperatures, short-term, local events are unlikely to have been dominant. A regional thermal
563 overprint on the passive margin sediments by warm ophiolite obduction can be excluded as the peak temperatures
564 in the Jebel Akhdar Dome are increasing with stratigraphic age. This is in agreement with models of Lutz et al.
565 (2004) outlining that even in subduction zones the isotherms of the rapidly buried sediments are not adjusting to
566 the surrounding temperatures instantaneously. Mon , the thermal imprint as observed by the metamorphic sole
567 in northern Oman is only affecting 10's of meters in the sub-thrust Hawasina Nappes (e.g. Searle and Cox, 2002)
568 and not the carbonate platform sediments below. This only minor sub-thrust thermal overprint is also observed in
569 other thrust zones (e.g. Wygrala, 1989).
570 To reach measured maturity data in the mountain area of the transect a paleo-thickness of the ophiolite in the order
571 of 8-10 km on top of 2 km of Hawasina Nappes is required (Figure 9); this would account for 280 to 320 MPa of lithostatic pressure and is in rough agreement with the pressure
572 reconstructed by combining fluid inclusion data and independently determined thermal rock maturity temperatures
573 (cf. FI results: 254 ± 30 MPa). Depending on lithological effects, such as a less pronounced serpentinization of the
574 ophiolite, this value might increase by up to 3 km (Figure 10). Basal heat flow values at deepest burial are estimated
575 to c. 40 mW/m². This seems realistic as passive margin conditions prevail, and no magmatism or rifting is reported
576 in the area.
577 Basin modeling indicates that highest temperatures were reached much later than deepest burial under the ophiolite
578 (Figure 7), dire  prior to uplift. This difference is interpreted as time the rock needed for thermal equilibration
579 after rapid burial. Deep burial under the ophiolite represents the only time in basin evolution when ductile
580 limestone deformation was possible (Grobe et al., 2018). However, there is uncertainty concerning the exact timing
581 of deepest burial in the Jebel Akhdar (we used 79 Ma according to U-Pb dating of eclogites in the Saih Hatat
582 window; Warren et al., 2005) and the beginning of early uplift (we used 55 Ma, as discussed below).
583 Our peak temperatures are in principal agreement with temperatures of c. 200 °C suggested for the top of the
584 carbonate platform by Breton et al. (2006) and non-reset zircon fission tracks in the pre-Permian basement
585 indicating peak temperatures up to 280 °C (Saddiqi et al., 2006). Moreover, thermal maturities of the same
586 stratigraphic units show similar values along the transect and around the dome (Grobe et al., 2016). Hence, we
587 assume a similar burial history for the entire Jebel Akhdar. However, a slightly deeper burial of the northern flank
588 can, within the range of error, not be excluded. The temperatures used in our models are in contrast with recent
589 results on mixed illite-smectite layers and clay mineral assemblages from the Jebel Akhdar by Aldega et al. (2017)
590 who argue for peak temperatures of 150-200 °C on the northern flank of the Jebel Akhdar and 120-150 °C on the
591 southern flank. These values are incompatible with our solid bitumen and Raman spectroscopy data, as well as
592 with the overmature Natih B source rock on the southern flank (data presented here and in Grobe et al. 2016).
593 Independent data on temperatures from fluid inclusions confirm the higher temperature range. At present, there is
594 no clear explanation for this discrepancy. However, it has been shown that the vitrinite reflectance system is more
595 sensitive to rapid temperature changes than clay mineralogy (e.g. Hillier et al., 1995; Velde and Lanson, 1993). If
596 burial was short enough, the clay minerals may not have time to recrystallize, possibly due to a lack of potassium,
597 whereas vitrinite reflectance increases. Another possible explanation may be that the dated clay minerals formed
598 during top-to-NNE shearing, a  us do not show peak burial. Indeed it has been shown that deformation
599 associated with this early extension reaches deeply into the passive margin sequence, and includes the Rayda and
600

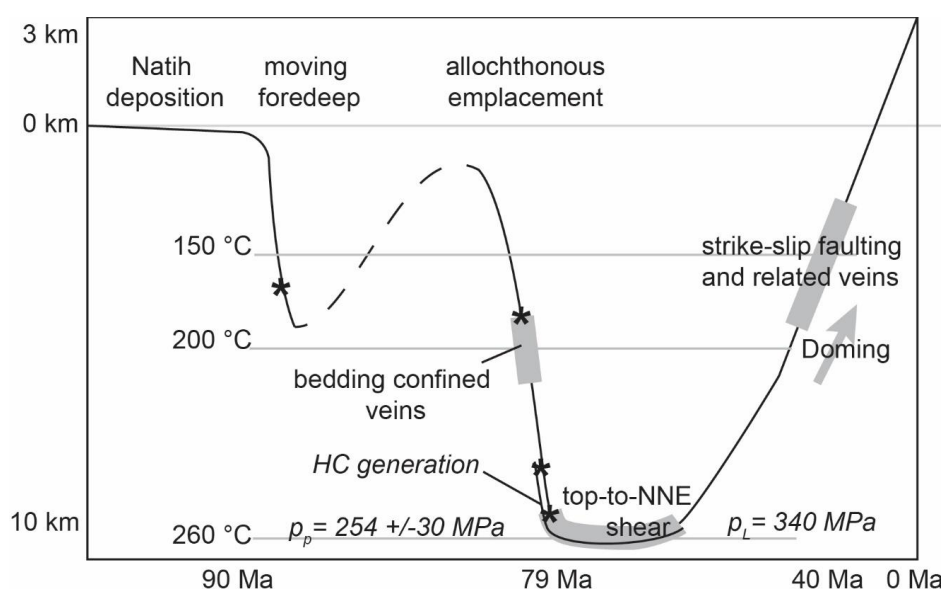


601 Shuaiba Formations (Grobe et al., 2018; Mattern and Scharf, 2018). Furthermore, Aldega et al. (2017) suggest that
 602 the thermal evolution during uplift of Grobe et al. (2016) does not account for thermochronological data in pre-
 603 Permian basement rocks (Poupeau et al., 1998; Saddiqi et al., 2006), arguing the 1D thermal models indicate
 604 temperature in the basement had to be lower than 70°C during the Eocene-Oligocene. In fact, the raw data from
 605 the basement indicate rapid cooling at 55 ± 5 Ma, in agreement with models of Grobe et al. (2016) and the
 606 exhumation presented in this work. 

607 Temperatures of the ductile top-to-NNE shearing event (64 ± 4 Ma, Hansman et al., 2018), marking the time of
 608 deepest burial and measured in bedding parallel veins, were reconstructed to 186–221 °C by Holland et al. (2009)
 609 assuming an ophiolitic overburden of 5 km (Saftan Fm., Wadi Nakhr). If we adjust this pressure correction for
 610 higher values of 280 to 340 MPa accounting for the here elaborated 8 to 10 km of ophiolite and 2 km of
 611 sedimentary nappes, trapping temperatures would increase to c. 296–364 °C (Table 3), which are in the order of
 612 the maximum burial temperatures as deduced from organic matter maturity. 

613 Figure 11 presents a summary burial plot indicating temperature and age constraints. Highlighted in gray is
 614 additional information gained by fluid inclusion thermometry. These data indicate paleo-fluid temperatures in the
 615 range of 225 ± 4 (280 MPa) to 266 ± 5 °C (340 MPa) during burial under the ophiolite (bedding-confined veins),
 616 c. 296–364 °C at peak burial (top-to-NNE sheared veins) and 213 ± 3 °C during exhumation with a later phase of
 617 primary inclusion outlining 184 ± 3 to 189 ± 7 °C (both strike-slip related veins). Temperature decrease within the
 618 latter formed parts of the strike-slip veins might relate to a change of fluid source or to exhumation during vein
 619 formation. In combination with our thermochronology data the second possibility appears more likely and would
 620 imply strike-slip faults developed after c. 55 Ma.

621



622
 623 Figure 11: Summary burial sketch for the top of the carbonate platform (Natih Fm.). Shown temperatures are based
 624 on RSCM and FI thermometry, pressure data calculated out of FI measurements and independently determined
 625 temperature data. The uplift history is restored by ZHe ages. (*) indicate times of overpressure formation, gray areas
 626 depict vein formation



627 **5.2. Exhumation history**

628 Our new thermochronology data from the central part of the Jebel Akhdar Dome suggests cooling below the reset
629 temperature of the ZHe thermochronometer (c. 170 °C) between 48.7 ± 1.8 and 39.8 ± 3.0 Ma (Table 2, Figure 4).
630 The small variation in cooling ages for the different stratigraphic levels indicates rapid passage of the entire rock
631 suite through the ZHe partial retention zone, and consequently rapid exhumation of the Jebel Akhdar Dome. This
632 Eocene cooling is in agreement with ZHe ages of pre-Permian strata of Hansman et al. (2017) ranging between 62
633 ± 3 and 39 ± 2 Ma. Apatite fission track (AFT) ages measured in the basement of the Jebel Akhdar range between
634 55 ± 5 Ma and 48 ± 7 Ma (4 samples, Poupeau et al. 1998) and 51 ± 8 Ma to 32 ± 4 Ma (Hansman et al., 2017).
635 The temperature of resetting the AFT system (i.e. the depth of the base of the partial annealing zone) may vary
636 depending on annealing kinetics. For different apatite crystals this temperature ranges between 100 and 120 °C
637 (Carlson et al., 1999; Fitzgerald et al., 2006). Hence, these AFT ages reproduce within error with our ZHe results,
638 despite the fact that both systems are sensitive to different temperature intervals (100-120 °C and 130-170 °C,
639 respectively). This supports the interpretation of rapid exhumation of the Jebel Akhdar. In combination with zircon
640 fission track ages of Saddiqi et al. (2006), indicating the rocks cooled below c. 260 °C between 70 and 96 Ma,
641 modeled cooling paths indicate rapid exhumation initiated at c. 55 Ma. Earlier exhumation would not result in
642 required thermal maturity.  Exposure of the rock to highest temperatures would be too short for thermal  equilibration. A reheating event in the late Miocene is not required to explain the data.

644

645 Our ZHe data from the Muti Formation and the Hawasina Nappes show a spread in ages, ranging from 43 to
646 173 Ma, i.e. partly much older than the ages observed in the stratigraphically lower units in the center of the dome.
647 This indicates the system has been only partially reset, implying these units were not heated above 170 °C after
648 deposition. Units exposed in the Hawasina Window (Figure 1) also show unreset ZHe ages (Csontos, pers. comm.).
649 The top of the Natih Formation has seen temperatures above 220 °C. We suggest this apparent contradiction may
650 be explained by juxtaposition of the colder Muti and Hawasina units against the top of the carbonate platform
651 during extensional top-to-NNE shearing. This implies that at least 50 °C of cooling are associated with post
652 obduction extension, i.e. before doming. A two-stage exhumation history of the Jebel Akhdar Dome has also been
653 inferred from structural data (Grobe et al., 2018; Mattern and Scharf, 2018) and the stratigraphic record (Fournier
654 et al., 2006; Mann et al., 1990).

655 **5.3. Pressure evolution and fluid migration**

656 Evolution of pore pressures was modelled (Figures S6 and S7 ~~Fehler! Verweisquelle konnte nicht gefunden werden.~~) assuming a perfect seal on top of the Natih Fm. ($k_{\text{Muti}} = 10^{-23} \text{ m}^2$). Porosity was lost during Muti deposition
657 in the moving forebulge (top seal) and related burial, the emplacement of the Hawasina Nappes and the ophiolite,
658 which induced compaction and a remaining very low porosity of c. 1 %. Hydrostatic pressure increased with the
659 moving forebulge at 88 Ma to 40 MPa, after Muti deposition to 60 MPa and after ophiolite emplacement to
660 120 MPa. Calculated pore pressure exceeded hydrostatic pressure in response to Hawasina Nappe and ophiolite
661 emplacement.
662 Formation of tensile fractures, as inferred from bedding confined, Mode-I veins in the Natih Fm. (Grobe et al.,
663 2018; e.g. Holland et al., 2009; Virgo, 2015), require internal fluid pressures (P_f) exceeding the sum of the stress
664 acting normal on the fracture surface (σ_3) and the tensile stress of the rock (T): $P_f > \sigma_3 + T$, and a differential
665



666 stress ($\sigma_1 - \sigma_3$) below 4T (Secor, 1965). Host-rock buffered vein isotope compositions indicate that the veins were
667 formed by local fluids (Arndt et al., 2014) and, hence, require local overpressure cells.
668 Sensitivity analyses of reduced permeabilities of Muti, Natih and Nahr Umr formations show that overpressure
669 generation, necessary for rock fracturing, requires a very good top seal and a reduced horizontal permeability of
670 the Natih Fm. of 10^{-23} m^2 (Figure S7). A top seal on its own is not sufficient for overpressures initiating rock
671 failure. This case results in pore pressures up to 300 MPa within the top Natih and localized overpressures of
672 195 MPa in front of the obducting ophiolite.
673 All results indicate that without low horizontal permeabilities of the Natih Fm. $\leq 10^{-23} \text{ m}^2$ overpressure cells
674 required for vein formation cannot be generated. The reduced permeabilities in the Natih Fm. are necessary to
675 prevent an early, tectonically-driven horizontal pressure release.

676 **5.4. Fluid migration**

677 Numerical basin modeling shows that rapid burial of sedimentary rocks below the ophiolite (88-80 Ma) caused
678 under-compaction, i.e. a porosity too high with respect to burial depth, and consequent pore pressure increase.
679 Two example model results of fluid migration in front of the obducting ophiolite are shown in the electronic
680 supplement Figure S8. If low permeabilities are assigned to the non-source-rock members of the Natih Fm.,
681 migration will mainly take place within the source rocks and at layer interfaces within the Natih Fm. If the complete
682 Natih Fm. has low permeabilities, fluids will leave the source rock vertically first, before lateral migration localizes
683 along layer boundaries. The pressure gradient between overpressures below the allochthonous nappes and the less
684 deeply buried southern foreland initiates tectonically-driven fluid migration in front of the obducting nappes, an
685 idea that was first introduced by Oliver (1986). Solid bitumen accumulations in black stained calcite veins are in
686 agreement with this interpretation (Fink et al., 2015).
687 Dome formation of the Jebel Akhdar anticline around 55 Ma initiated layer tilting and consequent northward
688 migration of the generated hydrocarbons as observed by secondary low reflective solid bitumen generations in
689 Natih veins and host rocks at the southern flank of the Oman Mountains (Fink et al., 2015; Grobe et al., 2016).

690 **6. Conclusions**

691 This study provides insights into the temperature evolution during obduction, prior to subsequent orogenesis.
692 Arabia's passive continental margin was buried to at least 4 km at times of foredeep migration and afterwards
693 under 8-10 km of Semail Ophiolite and 2 km of sedimentary Hawasina Nappes. Burial under the ophiolite resulted
694 in peak temperatures of up to 300 °C (Shu'aiba Fm.) with sub-lithostatic pore pressures. Ophiolite obduction and
695 overpressure cells expelled fluids towards the foreland, through matrix and fracture porosity.
696 ZHe data show cooling associated with forebulge migration, as well as with exhumation of the Jebel Akhdar Dome.
697 Exhumation of the Jebel Akhdar Dome took place in two stages. A first stage is associated with top-to-NNE
698 shearing, which is responsible for at least 50 °C of cooling, as witnessed by juxtaposition of units including
699 partially reset ZHe ages against units that experienced more than 220 °C. ZHe data show the second exhumation
700 phase, associated with doming of the Jebel Akhdar occurred between 49 and 39 Ma.



701 **Author contribution**

702 JLU, RL and AG conceived of the study. AG planned and carried out fieldwork as well as thermal maturity
703 measurements (VR, solid bitumen reflectance, Raman spectroscopy), structural interpretations and basin
704 modelling. CvH, JU and FW carried out fieldwork and structural interpretations. FW and ID conducted the
705 thermochronological measurements with help of CvH. PM and AG performed fluid inclusion thermometry.
706 AG and CvH prepared the manuscript with contributions from all co-authors.

707 **Acknowledgements**

708 We acknowledge the highly-appreciated help of Donka Macherey (sample preparation, RWTH Aachen), the team
709 of the KU Leuven (fluid inclusion measurements) and Keno Lünsdorf (Raman spectroscopy, Georg-August-
710 University, Göttingen). Sample crushing was realized by the team of SELFRAG, Switzerland. Wiekert Visser and
711 Victoria Sachse are thanked for fruitful discussions; Gösta Hoffmann and Wilfried Bauer thanked for helping with
712 field logistics. We are grateful for comments of Edwin Gnos, Andreas Scharf, Bruce Levell, Wolf-Christian Dullo
713 and Mark Handy on earlier versions of this manuscript.

714 **References**

715 Agard, P., Omrani, J., Jolivet, L. and Moutherieu, F.: Convergence history across Zagros (Iran): constraints from
716 collisional and earlier deformation, *International Journal of Earth Sciences*, 94(3), 401–419, doi:10.1007/s00531-
717 005-0481-4, 2005.

718 Al-Kindi, M. H. and Richard, P. D.: The main structural styles of the hydrocarbon reservoirs in Oman, *Geological
719 Society, London, Special Publications*, 392(1), 409–445, doi:10.1144/SP392.20, 2014.

720 Al-Lazki, A. I., Seber, D., Sandvol, E. and Barazangi, M.: A crustal transect across the Oman Mountains on the
721 eastern margin of Arabia, *GeoArabia*, 7(1), 47–78, 2002.

722 Al-Wardi, M. and Butler, R. W. H.: Constrictional extensional tectonics in the northern Oman mountains, its role
723 in culmination development and the exhumation of the subducted Arabian continental margin, *Geological Society,
724 London, Special Publication*, 272(1), 187–202, doi:10.1144/GSL.SP.2007.272.01.11, 2007.

725 Aldega, L., Carminati, E., Scharf, A., Mattern, F. and Al-Wardi, M.: Estimating original thickness and extent of
726 the Semail Ophiolite in the eastern Oman Mountains by paleothermal indicators, *Marine and Petroleum Geology*,
727 84, 18–33, doi:10.1016/j.marpetgeo.2017.03.024, 2017.

728 Aoya, M., Kouketsu, Y., Endo, S., Shimizu, H., Mizukami, T., Nakamura, D. and Wallis, S.: Extending the
729 applicability of the Raman carbonaceous-material geothermometer using data from contact metamorphic rocks,
730 *Journal of Metamorphic Geology*, 28(9), 895–914, doi:10.1111/j.1525-1314.2010.00896.x, 2010.

731 Arndt, M., Virgo, S., Cox, S. F. and Urai, J. L.: Changes in fluid pathways in a calcite vein mesh (Natih Fm, Oman
732 Mountains): insights from stable isotopes, *Geofluids*, 14(4), 391–418, doi:10.1111/gfl.12083, 2014.

733 Barker, C. E. E. and Pawlewicz, M. J. J.: Calculation of vitrinite reflectance from thermal histories and peak
734 temperatures, in *Vitrinite Reflectance as a Maturity Parameter*, vol. 570, edited by P. Mukhopadhyay and W. Dow,
735 pp. 216–229, American Chemical Society., 1994.

736 Béchenne, F., Metour, J. L. E., Rabu, D., Villey, M. and Beurrier, M.: The Hawasina Basin: A fragment of a
737 starved passive continental margin, thrust over the Arabian Platform during obduction of the Sumail Nappe,



738 Tectonophysics, 151(1–4), 323–343, doi:10.1016/0040-1951(88)90251-X, 1988.

739 Béchennec, F., Le Metour, J., Rabu, D., Bourdillon-de-Grissac, C., de Wever, P., Beurrier, M. and Villey, M.: The
740 Hawasina Nappes: stratigraphy, palaeogeography and structural evolution of a fragment of the south-Tethyan
741 passive continental margin, Geological Society, London, Special Publications, 49(1), 213–223,
742 doi:10.1144/GSL.SP.1992.049.01.14, 1990.

743 Bernoulli, D., Weissert, H. and Blome, C. D.: Evolution of the Triassic Hawasina Basin, Central Oman Mountains,
744 Geological Society, London, Special Publications, 49(1), 189–202, doi:10.1144/GSL.SP.1992.049.01.12, 1990.

745 Beurrier, M., Bechennec, F., Rabu, D. and Hutin, G.: Geological Map of Rustaq - explanatory notes, Sultanat of
746 Oman, Ministry of Petroleum and Minerals, 1986.

747 Beyssac, O., Goffé, B., Chopin, C. and Rouzaud, J. N.: Raman spectra of carbonaceous material in metasediments:
748 A new geothermometer, Journal of Metamorphic Geology, 20, 859–871, doi:10.1046/j.1525-1314.2002.00408.x,
749 2002.

750 Bodnar, R. J.: Revised equation and table for determining the freezing point depression of H₂O-NaCl solutions,
751 Geochimica et Cosmochimica Acta, 57, 683–684, 1993.

752 Breton, J. P., Béchennec, F., Le Métour, J., Moen-Maurel, L. and Razin, P.: Eoalpine (Cretaceous) evolution of
753 the Oman Tethyan continental margin: Insights from a structural field study in Jabal Akhdar (Oman Mountains),
754 GeoArabia, 9(2), 41–58, 2004.

755 Brown, P. E.: FLINCOR; a microcomputer program for the reduction and investigation of fluid-inclusion data,
756 American Mineralogist, 74, 1390–1393, 1989.

757 Van Buchem, F. S. P., Razin, P., Homewood, P. W., Philip, J. M., Eberli, G. P., Platel, J. P., Roger, J., Eschard,
758 R., Desaubliaux, G. M. J., Boisseau, T., Leduc, J. P., Labourdette, R. and Cantaloube, S.: High resolution sequence
759 stratigraphy of the Natih Formation (Cenomanian/Turonian) in northern Oman: distribution of source rocks and
760 reservoir facies, GeoArabia, 1(1), 65–91, 1996.

761 Van Buchem, F. S. P., Razin, P., Homewood, P. W., Oterdoom, W. H. and Philip, J.: Stratigraphic organization of
762 carbonate ramps and organic- rich intrashelf basins: Natih Formation (middle Cretaceous) of northern Oman,
763 AAPG Bulletin, 86(1), 21–53, doi:10.1306/61EEDA30-173E-11D7-8645000102C1865D, 2002.

764 Carlson, W. D., Donelick, R. A. and Ketcham, R. A.: Variability of apatite fission-track annealing kinetics: I.
765 Experimental results, American Mineralogist, 84(9), 1213–1223, doi:10.2138/am-1999-0901, 1999.

766 Claringbould, J. S., Hyden, B. B., Sarg, J. F. and Trudgill, B. D.: Structural evolution of a salt-cored, domed,
767 reactivated fault complex, Jebel Madar, Oman, Journal of Structural Geology, 51, 118–131,
768 doi:10.1016/j.jsg.2013.03.001, 2013.

769 Coleman, R. G.: Tectonic Setting for Ophiolite Obduction in Oman, Journal of Geophysical Research, 86(B4),
770 2497–2508, 1981.

771 Cooper, D. J. W., Ali, M. Y. and Searle, M. P.: Structure of the northern Oman Mountains from the Semail
772 Ophiolite to the Foreland Basin, Geological Society, London, Special Publications, 392, 129–153, 2014.

773 Cowan, R. J., Searle, M. P. and Waters, D. J.: Structure of the metamorphic sole to the Oman Ophiolite, Sumeini
774 Window and Wadi Tayyin: implications for ophiolite obduction processes, Geological Society, London, Special
775 Publications, 392(1), 155–175, doi:10.1144/SP392.8, 2014.

776 Deville, E. and Sassi, W.: Contrasting thermal evolution of thrust systems: An analytical and modeling approach
777 in the front of the western Alps, AAPG Bulletin, 90(6), 887–907, doi:10.1306/01090605046, 2006.

778 Duretz, T., Agard, P., Yamato, P., Ducassou, C. C., Burov, E. B. and Gerya, T. V.: Thermo-mechanical modeling



779 of the obduction process based on the Oman Ophiolite case, *Gondwana Research*, doi:10.1016/j.gr.2015.02.002,
780 2015.

781 Ferreiro Mählmann, R.: Correlation of very low grade data to calibrate a thermal maturity model in a nappe tectonic
782 setting, a case study from the Alps, *Tectonophysics*, 334, 1–33, 2001.

783 Filbrandt, J. B., Al-Dhahab, S., Al-Habsy, A., Harris, K., Keating, J., Al-mahruqi, S., Ozkaya, S. I., Richard, P. D.
784 and Robertson, T.: Kinematic interpretation and structural evolution of North Oman, Block 6, since the Late
785 Cretaceous and implications for timing of hydrocarbon migration into Cretaceous reservoirs, *GeoArabia*, 11(1),
786 97–115, 2006.

787 Fink, R., Virgo, S., Arndt, M., Visser, W., Littke, R. and Urai, J. L. L.: Solid bitumen in calcite veins from the
788 Natih Formation in the Oman Mountains: Multiple phases of petroleum migration in a changing stress field,
789 *International Journal of Coal Geology*, 157, 39–51, doi:10.1016/j.coal.2015.07.012, 2015.

790 Fitzgerald, P. G., Baldwin, S. L., Webb, L. E. and O’Sullivan, P. : He data from slowly cooled crustal terranes
791 and the interpretation of intra-sample variations of single crystal apatite ages from vertical profiles., *Chemical
792 Geology*, 225, 91–120, 2006.

793 Forbes, G. A., Jansen, H. S. M. and Schreurs, J.: Lexicon of Oman - Subsurface Stratigraphy - Reference Guide
794 to the Stratigraphy of Oman’s Hydrocarbon Basins, *GeoArabia* special publication 5, 2010.

795 Fournier, M., Lepvrier, C., Razin, P. and Jolivet, L.: Late Cretaceous to Paleogene post-obduction extension and
796 subsequent Neogene compression in the Oman Mountains, *GeoArabia*, 11(4), 17–40, 2006.

797 Glennie, K. W., Boeuf, M. G. A., Clarke, M. W. H., Moody-Stuart, M., Pilaar, W. F. H. and Reinhardt, B. M.:
798 Late Cretaceous Nappes in Oman Mountains and Their Geologic Evolution, *AAPG Bulletin*, 57(1), 5–27, 1973.

799 Glennie, K. W., Boeuf, M. G. A., Hughes Clarke, M. W., Moody-Stuart, M., Pilaar, W. F. H. and Reinhardt, B.
800 M.: Geology of the Oman Mountains, *Verhandelingen van het Koninklijk Nederlands geologisch mijnbouwkundig
801 Genootschap*, 31, 432, 1974.

802 Gnos, E. and Peters, T.: K-Ar ages of the metamorphic sole of the Semail Ophiolite: implications for ophiolite
803 cooling history, *Contributions to Mineralogy and Petrology*, 113, 325–332, 1993.

804 Goldstein, R. H.: Fluid inclusions in sedimentary and diagenetic systems, *Lithos*, 55(1–4), 159–193,
805 doi:10.1016/S0024-4937(00)00044-X, 2001.

806 Gomez-Rivas, E., Bons, P. D., Koehn, D., Urai, J. L., Arndt, M., Virgo, S., Laurich, B., Zeeb, C., Stark, L. and
807 Blum, P.: The Jabal Akhdar Dome in the Oman mountains: Evolution of a dynamic fracture system, *American
808 Journal of Science*, 314(7), 1104–1139, doi:10.2475/07.2014.02, 2014.

809 Grelaud, C., Razin, P., Homewood, P. W. and Schwab, a. M.: Development of Incisions on a Periodically
810 Emergent Carbonate Platform (Natih Formation, Late Cretaceous, Oman), *Journal of Sedimentary Research*,
811 76(4), 647–669, doi:10.2110/jsr.2006.058, 2006.

812 Grobe, A., Littke, R., Urai, J. L. and Lünsdorf, N. K.: Hydrocarbon generation and migration under a large
813 overthrust: The carbonate platform under the Semail Ophiolite, Jebel Akhdar, Oman, *International Journal of Coal
814 Geology*, 168, 3–19, doi:10.1016/j.coal.2016.02.007, 2016.

815 Grobe, A., Virgo, S., von Hagke, C., Urai, J. L. and Littke, R.: Multiphase Structural Evolution of a Continental
816 Margin During Obduction Orogeny: Insights From the Jebel Akhdar Dome, Oman Mountains, *Tectonics*, 37(3),
817 888–913, doi:10.1002/2016TC004442, 2018.

818 Guenther, W. R., Reiners, P. W., Ketcham, R. A., Nasdala, L. and Giester, G.: *American Journal of Science*,
819 *American Journal of Science*, 313(March), 145–198, doi:10.2475/03.2013.01, 2013.



820 Habsi, N. Al, Shukaili, M. Al, Tooqi, S. Al, Ehrenberg, S. N. and Bernecker, M.: Lithofacies, diagenesis and
821 reservoir quality of Upper Shu'aiba reservoirs in northwestern Oman, *GeoArabia*, 19(4), 145–182, 2014.

822 Hacker, B. R. and Mosenfelder, J. L.: Metamorphism and deformation along the emplacement thrust of the Samail
823 ophiolite, Oman, *Earth and Planetary Science Letters*, 144(3–4), 435–451, doi:10.1016/S0012-821X(96)00186-0,
824 1996.

825 Hacker, B. R., Mosenfelder, J. L. and Gnos, E.: Rapid emplacement of the Oman ophiolite: Thermal and
826 geochronologic constraints, *Tectonics*, 15(6), 1230–1247, 1996.

827 Hanna, S. S.: The Alpine deformation of the Central Oman Mountains, Geological Society, London, Special
828 Publications, 49(1), 341–359, doi:10.1144/GSL.SP.1992.049.01.21, 1990.

829 Hansman, R. J., Ring, U., Thomson, S. N. and Brok, B. Den: Late Eocene uplift of the Al Hajar Mountains, Oman,
830 supported by stratigraphy and low-temperature thermochronology, *Tectonics*, doi:10.1002/2017TC004672, 2017.

831 Hansman, R. J., Albert, R., Gerdes, A. and Ring, U.: Absolute ages of multiple generations of brittle structures by
832 U-Pb dating of calcite, *Geology*, doi:10.1130/G39822.1, 2018.

833 Hassanzadeh, J. and Wernicke, B. P.: The Neotethyan Sanandaj-Sirjan zone of Iran as an archetype for passive
834 margin-arc transitions, *Tectonics*, 25(3), 586–621, doi:10.1002/2015TC003926, 2016.

835 Hilgers, C., Kirschner, D. L., Breton, J. P. P. and Urai, J. L.: Fracture sealing and fluid overpressures in limestones
836 of the Jabal Akhdar dome, Oman mountains, *Geofluids*, 6(2), 168–184, doi:10.1111/j.1468-8123.2006.00141.x,
837 2006.

838 Hillier, S., Mátyás, J., Matter, A. and Vasseur, G.: Illite/smectite diagenesis and its variable correlation with
839 vitrinite reflectance in the Pannonian Basin, *Clays and Clay Minerals*, 43(2), 174–183,
840 doi:10.1346/CCMN.1995.0430204, 1995.

841 Holland, M., Urai, J. L., Muchez, P. and Willemse, E. J. M.: Evolution of fractures in a highly dynamic thermal,
842 hydraulic, and mechanical system - (I) Field observations in Mesozoic Carbonates, Jabal Shams, Oman Mountains,
843 *GeoArabia*, 14(1), 57–110, 2009.

844 Homewood, P., Razin, P., Grélaud, C., Droste, H., Vahrenkamp, V., Mettraux, M. and Mattner, J.: Outcrop
845 sedimentology of the Natih Formation, northern Oman: A field guide to selected outcrops in the Adam Foothills
846 and Al Jabal al Akhdar areas, *GeoArabia*, 13(3), 39–120, 2008.

847 Immenhauser, A. and Scott, R. W.: An estimate of Albian sea-level amplitudes and its implication for the duration
848 of stratigraphic hiatuses, *Sedimentary Geology*, 152(1–2), 19–28, doi:10.1016/S0037-0738(02)00260-9, 2002.

849 Immenhauser, A., Schlager, W., Burns, S. J., Scott, R. W., Geel, T., Lehmann, J., van der Gaast, S. and Bolder-
850 Schrijver, L. J. A. J. a.: Late Aptian to late Albian sea-level fluctuations constrained by geochemical and biological
851 evidence (Nahr Umr Formation, Oman), *Journal of Sedimentary Research*, 69(2), 434–446,
852 doi:10.2110/jsr.69.434, 1999.

853 Jacobs, J., Thomas, R. J., Ksienzyk, A. K. and Dunkl, I.: Tracking the Oman Ophiolite to the surface - New fission
854 track and (U-Th)/He data from the Aswad and Khor Fakkan Blocks, UAE, *Tectonophysics*, 644, 68–80,
855 doi:10.1016/j.tecto.2014.12.018, 2015.

856 De Keijzer, M., Hillgartner, H., Al Dhahab, S. and Rawnsley, K.: A surface-subsurface study of reservoir-scale
857 fracture heterogeneities in Cretaceous carbonates, North Oman, Geological Society, London, Special Publications,
858 270(1), 227–244, doi:10.1144/GSL.SP.2007.270.01.15, 2007.

859 Ketcham, R. A.: Forward and Inverse Modeling of Low-Temperature Thermochronometry Data, *Reviews in*
860 *Mineralogy and Geochemistry*, 58, 275–314, doi:10.2138/rmg.2005.58.11, 2005.



861 Koehler, B., Zeller, M., Aigner, T., Poeppelreiter, M., Milroy, P., Forke, H. and Al-Kindi, S.: Facies and
862 stratigraphic framework of a Khuff outcrop equivalent: Saiq and Mahil formations, Al Jabal al-Akhdar, Sultanate
863 of Oman, *GeoArabia*, 15(2), 91–156, 2010.

864 Koehler, B., Aigner, T. and Poppelreiter, M.: Field-scale geometries of Upper Khuff reservoir geobodies in an
865 outcrop analogue (Oman Mountains, Sultanate of Oman), *Petroleum Geoscience*, 17(1), 3–16, doi:10.1144/1354-
866 079310-009, 2011.

867 Kouketsu, Y., Mizukami, T., Mori, H., Endo, S., Aoya, M., Hara, H., Nakamura, D. and Wallis, S.: A new approach
868 to develop the Raman carbonaceous material geothermometer for low-grade metamorphism using peak width,
869 *Island Arc*, 23, 33–50, doi:10.1111/iar.12057, 2014.

870 Lippard, S. J., Smewing, J. D., Rothery, D. a. and Browning, P.: The geology of the Dibba zone, northern Oman
871 mountains - a preliminary study, *Journal of the Geological Society*, 139(1), 59–66, doi:10.1144/gsjgs.139.1.0059,
872 1982.

873 Loosveld, R. J. H., Bell, A. and Terken, J. J. M.: The Tectonic Evolution of Interior Oman, *GeoArabia*, 1(1), 28–
874 51, 1996.

875 Lünsdorf, N. K.: Raman spectroscopy of dispersed vitrinite - methodical aspects and correlation with reflectance,
876 *International Journal of Coal Geology*, 153(1), 75–86, doi:10.1016/j.coal.2015.11.010, 2016.

877 Lünsdorf, N. K., Dunkl, I., Schmidt, B. C., Rantitsch, G. and von Eynatten, H.: The thermal history of the Steinach
878 Nappe (eastern Alps) during extension along the Brenner Normal Fault system indicated by organic maturation
879 and zircon (U-Th)/ He thermochronology, *Austrian Journal of Earth Sciences*, 105(3), 17–25, 2012.

880 Lutz, R., Littke, R., Gerling, P. and Bönnemann, C.: 2D numerical modelling of hydrocarbon generation in
881 subducted sediments at the active continental margin of Costa Rica, *Marine and Petroleum Geology*, 21(6), 753–
882 766, doi:10.1016/j.marpetgeo.2004.03.005, 2004.

883 Mann, a., Hanna, S. S. and Nolan, S. C.: The post-Campanian tectonic evolution of the Central Oman Mountains:
884 Tertiary extension of the Eastern Arabian Margin, *The Geology and Tectonics of the Oman Region*, 49(1), 549–
885 563, doi:10.1144/gsl.sp.1992.049.01.33, 1990.

886 Mattern, F. and Scharf, A.: Postobductional extension along and within the Frontal Range of the Eastern Oman
887 Mountains, *Journal of Asian Earth Sciences*, 2, 154, doi:10.1016/j.jseaes.2017.12.031, 2018.

888 Le Metour, J., Rabu, D., Tegyey, M., Bechenne, F., Beurrier, M. and Villey, M.: Subduction and obduction: two
889 stages in the EoAlpine tectonometamorphic evolution of the Oman Mountains, *Geological Society, London,*
890 *Special Publications*, 49(1), 327–339, doi:10.1144/GSL.SP.1992.049.01.20, 1990.

891 Mount, V. S., Crawford, R. I. S., Bergmann, S. C. and Bergman, S. C.: Regional Structural Style of the Central
892 and Southern Oman Mountains: Jebel Akhdar, Saih Hatat, and the Northern Ghaba Basin, *GeoArabia*, 3(4), 17,
893 1998.

894 Moutherneau, F.: Timing of uplift in the Zagros belt/Iranian plateau and accommodation of late Cenozoic Arabia -
895 Eurasia convergence, *Geological Magazine*, 148(5–6), 726–738, doi:10.1017/S0016756811000306, 2011.

896 Mozafari, M., Swennen, R., Balsamo, F., Clemenzi, L., Storti, F., El Desouky, H., Vanhaecke, F., Tueckmantel,
897 C., Solum, J. and Taberner, C.: Paleofluid Evolution In Fault-Damage Zones: Evidence From Fault-Fold
898 Interaction Events In the Jabal Qusaybah Anticline (Adam Foothills, North Oman), *Journal of Sedimentary*
899 *Research*, 85(12), 1525–1551, doi:10.2110/jsr.2015.95, 2015.

900 Muchez, P., Marshall, J. D., Touret, J. L. R. and Viaene, W. a.: Origin and migration of palaeofluids in the Upper
901 Visean of the Campine Basin, northern Belgium, *Sedimentology*, 41(1), 133–145, doi:10.1111/j.1365-



902 3091.1994.tb01395.x, 1994.

903 Neumaier, M.: Structural Restoration and Basin and Petroleum Systems Modeling: Case Studies from the Monagas

904 Fold and Thrust Belt, Venezuela and the Moroccan Atlantic Margin, Dissertation, RWTH Aachen University.,

905 2015.

906 Nolan, S. C., Skelton, P. W., Clissold, B. P. and Smewing, J. D.: Maastrichtian to early Tertiary stratigraphy and

907 palaeogeography of the Central and Northern Oman Mountains, Geological Society, London, Special Publications,

908 49(1), 495–519, doi:10.1144/gsl.sp.1992.049.01.31, 1990.

909 Nöth, S., Karg, H. and Littke, R.: Reconstruction of Late Paleozoic heat flows and burial histories at the

910 Rhenohercynian-Subvariscan boundary, Germany, International Journal of Earth Sciences, 90(2), 234–256,

911 doi:10.1007/s005310000114, 2001.

912 Oliver, J.: Fluids expelled tectonically from orogenic belts: Their role in hydrocarbon migration and other geologic

913 phenomena, Geology, 14(February), 99–102, 1986.

914 Oxburgh, E. R. and Turcotte, D. L.: Thermal gradients and regional metamorphism in overthrust terrains with

915 special reference to the Eastern Alps, Schweizerische Mineralogische und Petrographische Mitteilungen, 54(2/3),

916 642–662, 1974.

917 Philip, J., Borgoman, J. and Al-Maskiry, S.: Cenomanian-Early Turonian carbonate platform of Northern Oman:

918 stratigraphy and palaeo-environments, Palaeogeography, Palaeoclimatology, Palaeoecology, 119, 77–92, 1995.

919 Pöppelreiter, M. C., Schneider, C. J., Obermaier, M., Forke, H. C., Koehrer, B. and Aigner, T.: Seal turns into

920 reservoir: Sudair equivalents in outcrops, A1 Jabal al-Akhdar, Sultanate of Oman, GeoArabia, 16(1), 69–108,

921 2011.

922 Poupeau, G., Saddiqi, O., Michard, A., Goffé, B. and Oberhänsli, R.: Late thermal evolution of the Oman

923 Mountains subophiolitic windows: Apatite fission-track thermochronology, Geology, 26(12), 1139–1142, 1998.

924 Pratt, R., Smewing, D., Swansea, S. A., Pratt, B. R. and Smewing, J. D.: Jurassic and Early Cretaceous platform

925 margin configuration and evolution, central Oman Mountains, Geological Society, London, Special Publications,

926 49(1), 69–88, doi:10.1144/GSL.SP.1992.049.01.06, 1990.

927 Rabu, D., Le Metour, J., Bechenne, F., Beurrier, M., Villey, M. and Bourdillon-Jeudy de Grissac, C.: Sedimentary

928 aspects of the Eo-Alpine cycle on the northeast edge of the Arabian Platform (Oman Mountains), Geological

929 Society, London, Special Publications, 49(1), 49–68, doi:10.1144/GSL.SP.1992.049.01.05, 1990.

930 Rantitsch, G. and Rainer, T.: Thermal modeling of Carboniferous to Triassic sediments of the Karawanken Range

931 (Southern Alps) as a tool for paleogeographic reconstructions in the Alpine-Dinaridic-Pannonian realm,

932 International Journal of Earth Sciences, 92(2), 195–209, doi:10.1007/s00531-003-0312-4, 2003.

933 Reiners, P. W.: Zircon (U-Th)/He Thermochronometry, Reviews in Mineralogy and Geochemistry, 58(1936),

934 151–179, doi:10.2138/rmg.2005.58.6, 2005.

935 Reutter, K.-J., Teichmüller, M. and Teichmüller, R.: The Coalification Pattern in the Northern Apennines and its

936 Palaeogeothermic and Tectonic Significance, Geologische Rundschau/Geologische Rundschau, 72(3), 861–894,

937 1988.

938 Rioux, M., Bowring, S., Kelemen, P., Gordon, S., Miller, R. and Dudás, F.: Tectonic development of the Samail

939 ophiolite: High-precision U-Pb zircon geochronology and Sm-Nd isotopic constraints on crustal growth and

940 emplacement, Journal of Geophysical Research: Solid Earth, 118(5), 2085–2101, doi:10.1002/jgrb.50139, 2013.

941 Rioux, M., Garber, J., Bauer, A., Bowring, S., Searle, M., Kelemen, P. and Hacker, B.: Synchronous formation of

942 the metamorphic sole and igneous crust of the Semail ophiolite: New constraints on the tectonic evolution during



943 ophiolite formation from high-precision U–Pb zircon geochronology, *Earth and Planetary Science Letters*, 451,
944 185–195, doi:10.1016/j.epsl.2016.06.051, 2016.

945 Robertson, A.: The transition from a passive margin to an Upper Cretaceous foreland basin related to ophiolite
946 emplacement in the Oman Mountains, *Geological Society of America Bulletin*, 99, 633–653, doi:10.1130/0016-
947 7606(1987)99<633, 1987.

948 Rolandone, F., Lucaleau, F., Leroy, S., Mareschal, J.-C., Jorand, R., Goutorbe, B. and Bouquerel, H.: New heat
949 flow measurements in Oman and the thermal state of the Arabian Shield and Platform, *Tectonophysics*, 589, 77–
950 89, doi:10.1016/j.tecto.2012.12.034, 2013.

951 Roure, F., Andriessen, P., Callot, J. P., Faure, J. L., Ferket, H., Gonzales, E., Guilhaumou, N., Lacombe, O.,
952 Malandain, J., Sassi, W., Schneider, F., Swennen, R. and Vilasi, N.: The use of palaeo-thermo-barometers and
953 coupled thermal, fluid flow and pore-fluid pressure modelling for hydrocarbon and reservoir prediction in fold and
954 thrust belts, *Geological Society, London, Special Publications*, 348(1), 87–114, doi:10.1144/SP348.6, 2010.

955 Saddiqi, O., Michard, A. N., Goffe, B. R., Poupeau, G. É. and Oberhansli, R. O.: Fission-track thermochronology
956 of the Oman Mountains continental windows, and current problems of tectonic interpretation, *Bull. Soc. géol. Fr.*,
957 177(3), 127–134, doi:10.2113/gssgbull.177.3.127, 2006.

958 Scott, R. W.: Chronostratigraphy of the Cretaceous carbonate shelf, southeastern Arabia, *Geological Society,*
959 *London, Special Publications*, 49(1), 89–108, doi:10.1144/GSL.SP.1992.049.01.07, 1990.

960 Searle, M. P.: Sequence of thrusting and origin of culminations in the northern and central Oman Mountains,
961 *Journal of Structural Geology*, 7(2), 129–143, doi:10.1016/0191-8141(85)90127-0, 1985.

962 Searle, M. P.: Structural geometry, style and timing of deformation in the Hawasina Window, Al Jabal al Akhdar
963 and Saih Hatat culminations, Oman Mountains, *GeoArabia*, 12(2), 99–130, 2007.

964 Searle, M. P. and Cox, J. O. N.: Subduction zone metamorphism during formation and emplacement of the Semail
965 ophiolite in the Oman Mountains, *Geological Magazine*, 139(3), 241–255, doi:10.1017/S0016756802006532,
966 2002.

967 Searle, M. P., Warren, C. J., Waters, D. J. and Parrish, R. R.: Subduction zone polarity in the Oman Mountains:
968 implications for ophiolite emplacement, *Geological Society, London, Special Publications*, 218(1), 467–480,
969 doi:10.1144/GSL.SP.2003.218.01.24, 2003.

970 Searle, M. P., Warren, C. J. J., Waters, D. . J. and Parrish, R. . R.: Structural evolution, metamorphism and
971 restoration of the Arabian continental margin, Saih Hatat region, Oman Mountains, *Journal of Structural Geology*,
972 26(3), 451–473, doi:10.1016/j.jsg.2003.08.005, 2004.

973 Secor, D. T. jr.: Role of fluid pressure in jointing, *American Journal of Science*, 263(October), 633–646, 1965.

974 Stenhouse, P.: Reactive Transport and Fluid Pathways in Fracture-Controlled Flow Systems, (Doctoral
975 Dissertation), Australian National University., 2014.

976 Sweeney, J. J. and Burnham, A. K.: Evaluation of a Simple Model of Vitrinite Reflectance Based on Chemical
977 Kinetics, *The American Association of Petroleum Geologists Bulletin*, 74(10), 1559–1570, 1990.

978 Teichmüller, R. and Teichmüller, M.: Relations between coalification and palaeogeothermics in Variscan and
979 Alpidic foredeeps of western Europe, *Lecture Notes in Earth Sciences*, 5, 1986.

980 Terken, J. M. J.: The Natih petroleum system of north Oman, *GeoArabia*, 4(2), 157–180, 1999.

981 Terken, J. M. J., Frewin, N. L., Indrelid, S. L. and Indrelin, S. L.: Petroleum systems of Oman: Charge timing and
982 risks, *AAPG Bulletin*, 85(10), 1817–1845, 2001.

983 Vahrenkamp, V. C.: Chemostratigraphy of the Lower Cretaceous Shu'aiba Formation: A delta-13C reference



984 profile for the Aptian Stage from the southern Neo-Tethys Ocean, *GeoArabia*, 1, 107–137, 2010.

985 Velde, B. and Lanson, B.: Comparison of I/S transformation and maturity of organic matter at elevated
986 temperatures, *Clays and Clay Minerals*, 41(2), 178–183, 1993.

987 Virgo, S.: Aspects of crack-seal vein system evolution. (Doctoral Dissertation). Retrieved from <http://nbn-resolving.de/urn/resolver.pl?urn=urn:nbn:de:hbz:82-opus-33858.>, RWTH Aachen University., 2015.

988 Virgo, S. and Arndt, M.: Evolution of a crack-seal calcite vein network in limestone: a high resolution structural,
989 microstructural and geochemical study from the Jebel Akhdar high pressure cell, Oman Mountains, (Diploma
990 Thesis.), RWTH Aachen [online] Available from: <http://darwin.bth.rwth-aachen.de/opus3/volltexte/2010/3385/>,
991 2010.

992 Virgo, S., Arndt, M., Sobisch, Z. Z. and Urai, J. L.: Development of fault and vein networks in a carbonate
993 sequence near Hayl al-Shaz, Oman Mountains, *GeoArabia*, 18(2), 99–136 [online] Available from:
994 <http://www.gulfpetrolink.net/publication/vol18.php>, 2013.

995 Visser, W.: Burial and thermal history of Proterozoic source rocks in Oman, *Precambrian Research*, 54(1), 15–36,
996 doi:10.1016/0301-9268(91)90066-J, 1991.

997 Warburton, J., Burnhill, T. J., Graham, R. H. and Isaac, K. P.: The evolution of the Oman Mountains Foreland
998 Basin, *The Geology and Tectonics of the Oman Region*, 49(1), 419–427, doi:10.1144/GSL.SP.1992.049.01.26,
999 1990.

1000 Warren, C. J., Parrish, R. R., Searle, M. P. and Waters, D. J.: Dating the subduction of the Arabian continental
1001 margin beneath the Semail ophiolite, Oman, *Geology*, 31(10), 889, doi:10.1130/G19666.1, 2003.

1002 Warren, C. J., Parrish, R. R., Waters, D. J. and Searle, M. P.: Dating the geologic history of Oman's Semail
1003 ophiolite: insights from U-Pb geochronology, *Contributions to Mineralogy and Petrology*, 150(4), 403–422,
1004 doi:10.1007/s00410-005-0028-5, 2005.

1005 Wygrala, B. P.: Integrated study on an oil field in the southern po basin, northern italy, *Berichte der
1006 Kernforschungsanlage Jülich*, 2313(October), 217, 1989.

1007

1008